RSC Advances

REVIEW

View Article Online
View Journal | View Issue

Cite this: *RSC Adv.*, 2025, **15**, 24696

Molecular imaging using (nano)probes: cutting-edge developments and clinical challenges in diagnostics

Meisam Samadzadeh,[a] Arezoo Khosravi,[bc] Atefeh Zarepour,[de] Ghazaleh Jamalipour Soufi,*[f] Ali Hekmatnia,[f] Ali Zarrabi *[g] and Siavash Iravani *[h]

Molecular imaging has emerged as a transformative approach in the field of medical diagnostics, enabling the visualization of biological processes at the molecular and cellular levels. Additionally, the integration of molecular imaging with other imaging modalities such as positron emission tomography (PET), magnetic resonance imaging (MRI), computed tomography (CT), photoacoustic imaging (PAI), and fluorescence imaging (FI) has further broadened the scope of diagnostics. Despite significant advances in probe design, including multifunctional and targeted nanomaterials, their clinical translation remains limited by critical challenges. Key obstacles include nanoprobe stability in physiological environments, nonspecific accumulation in the reticuloendothelial system, potential toxicity, and difficulties in achieving optimal biocompatibility and controlled biodistribution. Moreover, the complexity of nanoprobe synthesis and batch-to-batch variability hinder scalable manufacturing and regulatory approval. The primary goal of this review is to critically analyze the current challenges hindering the clinical translation of molecular imaging nanoprobes in biomedicine. While existing literature extensively covers imaging techniques, this review uniquely emphasizes the persistent obstacles—such as nanoprobe stability, biocompatibility, off-target effects, and limited sensitivity—that impede their effective application. Unlike previous reviews, which tend to focus broadly on advancements, we offer a nuanced perspective by identifying specific barriers and proposing promising strategies to overcome them. We explore how surface modification, novel targeting ligands, and smart responsive systems can enhance nanoprobe performance. Furthermore, the review discusses how addressing these challenges is crucial for accelerating the development of multifunctional nanoprobes capable of simultaneous diagnosis and therapy, ultimately advancing personalized medicine. By highlighting these hurdles and potential solutions, this review aims to provide a comprehensive roadmap for researchers striving to optimize molecular imaging nanoprobes, thereby bridging the gap between laboratory innovation and clinical reality.

Received 3rd June 2025
Accepted 7th July 2025

DOI: 10.1039/d5ra03927d

rsc.li/rsc-advances

1 Introduction

Molecular imaging is an advanced medical imaging technique which enables monitoring biological processes at both cellular and subcellular levels, facilitating early and noninvasive diagnosis, especially in the case of tumor visualization (Fig. 1).[1,2] Chemosynthetic probes, commonly used in molecular imaging, typically comprise two functional modules: an imaging module that generates detectable signals and a targeting module that specifically binds to lesion sites or interacts with molecules. Although these probes enhance imaging resolution at the molecular level, they raise biosafety concerns, including potential chemical toxicity.[3] Building on this foundation, molecular imaging probes have evolved through the integration of multidisciplinary advancements to meet the demands of clinical applications. Molecular imaging has become a vital tool in clinical diagnosis, leveraging advanced modalities such as positron emission tomography (PET), magnetic resonance

[a]*Department of Molecular Biology and Genetics, Faculty of Engineering and Natural Sciences, Istinye University, Istanbul 34396, Türkiye*
[b]*Department of Genetics and Bioengineering, Faculty of Engineering and Natural Sciences, Istanbul Okan University, Istanbul 34959, Türkiye*
[c]*Graduate School of Biotechnology and Bioengineering, Yuan Ze University, Taoyuan 320315, Taiwan*
[d]*Department of Biology, Faculty of Arts and Sciences, Kocaeli University, 41001, İzmit, Kocaeli, Türkiye*
[e]*Department of Research Analytics, Saveetha Dental College and Hospitals, Saveetha Institute of Medical and Technical Sciences, Saveetha University, Chennai – 600 077, India*
[f]*Radiology Department, School of Medicine, Isfahan University of Medical Science, Isfahan, Iran. E-mail: ghazalehsoofi@gmail.com*
[g]*Department of Biomedical Engineering, Faculty of Engineering and Natural Sciences, Istinye University, Istanbul 34396, Türkiye. E-mail: alizarrabi@gmail.com*
[h]*Independent Researcher, W Nazar ST, Boostan Ave, Isfahan, Iran. E-mail: siavashira@gmail.com*

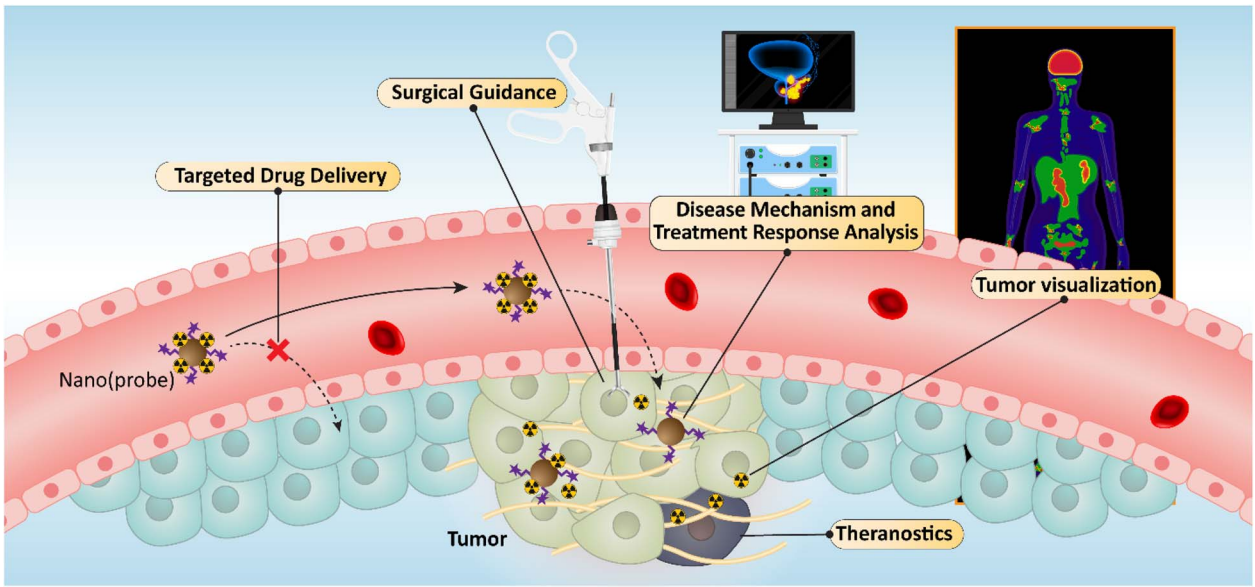

Fig. 1 Schematic illustration of multifunctional roles of molecular imaging probes in cancer diagnosis and therapy. Nano(probes) are shown crossing the vascular barrier to target tumor tissue, enabling tumor visualization, theranostics, surgical guidance, disease mechanism study, treatment response monitoring, and targeted drug delivery.

imaging (MRI), computed tomography (CT), photoacoustic imaging (PAI), and fluorescence imaging (FI). These techniques rely on molecular (nano)probes to generate imaging signals. For clinical applications, an ideal molecular imaging probe must exhibit high affinity, selectivity, stability, and cost-effective production. The development of imaging probes requires a multidisciplinary approach, integrating expertise from chemistry, biology, pharmaceuticals, radiochemistry, and clinical sciences.[4]

MRI molecular (nano)probes have developed medical diagnostics by enabling targeted, high-resolution imaging of biological processes at the molecular level.[5] Recent advancements include the development of nanoparticle (NP)-based probes that enhance contrast and facilitate theranostics, allowing for simultaneous imaging and targeted therapy. However, challenges such as the need for highly specific and biocompatible probes, as well as complex regulatory pathways for approval, remain significant hurdles. Additional explorations are expected to focus on creating sophisticated probes with advanced targeting strategies, leveraging machine learning and artificial intelligence (AI) for better data interpretation, and enhancing the diagnostic capabilities of MRI while improving patient outcomes and personalizing medical care.[5,6] Additionally, PET molecular probes have significantly advanced medical imaging by enabling the visualization of metabolic processes and enhancing diagnostic accuracy, particularly in cancer detection.[7] Recent developments focus on creating more specific probes that target disease-related receptors and novel radiotracers for diverse biological processes, as well as integrating PET with other imaging modalities like MRI and CT for comprehensive assessments. However, challenges such as the need for specialized facilities to produce radiolabeled compounds, the short half-life of radionuclides, and high costs can limit accessibility and widespread clinical implementation. Looking forward, innovations in radiochemistry, the possibility of new radionuclides, and the incorporation of AI for improved image analysis hold promise for refining PET molecular probes.[7,8] On the other hand, CT molecular probes have enhanced the diagnostic capabilities of CT imaging by enabling targeted visualization of specific biological processes and disease markers, primarily through the use of advanced contrast agents, including nanoparticles (NPs) and biodegradable polymers.[9] Recent advancements emphasize the development of targeted probes (Table 1) that improve tumor detection and the integration of CT with other imaging modalities like PET and MRI for comprehensive assessments. However, challenges remain, including potential adverse reactions to contrast agents, concerns over radiation exposure, and the need for safer imaging protocols. However, the future of CT molecular probes appears promising, with research focused on creating next-generation contrast agents that enhance safety and efficacy, as well as leveraging AI to improve image analysis.[9,10]

Photoacoustic molecular imaging (nano)probes are advancing medical imaging by combining the high spatial resolution of optical imaging with the deep tissue penetration of ultrasound, allowing for real-time visualization of molecular and cellular processes.[20] Recent developments include the development of novel nanomaterials, such as gold (Au) NPs and organic dyes, which enhance signal intensity and targeting capabilities, as well as the ability to perform multiplexed imaging to visualize multiple targets simultaneously. However, challenges remain in the clinical translation of these probes, including the need for standardized protocols, limited penetration depth compared to traditional imaging modalities, and concerns about reproducibility and long-term stability. The future of photoacoustic imaging is promising, with ongoing

Table 1 Different types of targeting ligands used for molecular imaging and theranostics

Ligand type	Specificity	Stability	Immunogenicity	Cost	Size	Ease of modification	Ref.
Antibodies	Very high	Moderate (can degrade *in vivo*)	Moderate to high (especially full-length antibodies)	High	~150 kDa (IgG)	Moderate (requires genetic or chemical conjugation)	11 and 12
Peptides	High	Moderate to high	Low	Moderate	1–5 kDa	High (amenable to chemical synthesis)	13 and 14
Aptamers	High	High (especially DNA aptamers)	Very low	Low to moderate	~5–25 kDa	Very high (*via* SELEX and chemical synthesis)	15–17
Small molecules	Moderate to high	High	Very low	Low	<1 kDa	Very high	18 and 19

research focused on creating more sophisticated, multifunctional probes and integrating advanced imaging systems and AI for improved image analysis.[20,21] Additionally, fluorescence molecular imaging probes have emerged as a powerful tool for visualizing biological processes at the molecular and cellular levels, providing high sensitivity and specificity in applications such as cancer diagnostics and surgical guidance (Fig. 1).[22,23] Current explorations include the development of activatable probes that enhance contrast by emitting fluorescence only in the presence of specific biomarkers, as well as the use of NPs and quantum dots for improved brightness and stability. However, challenges such as tissue auto-fluorescence, limited tissue penetration of visible light, and regulatory hurdles can complicate implementation in clinical settings. It appears that fluorescence molecular imaging holds promise with ongoing research focused on creating next-generation probes with multifunctional capabilities and the integration of AI for enhanced image analysis, ultimately aiming to facilitate better disease diagnosis and personalized medicine.[22,24]

Recent advancements in the design of these molecular imaging probes have focused on improving their biocompatibility, stability, and targeting efficiency. For instance, the incorporation of functionalized NPs—such as Au, silica, and liposomes—has demonstrated enhanced imaging contrast and longer circulation times in biological systems.[25,26] Additionally, the use of multifunctional (nano)probes that combine imaging and therapeutic capabilities, known as theranostic agents, is gaining traction. These probes not only facilitate visualization of disease states but also enable targeted drug delivery (Fig. 1), thus improving treatment efficacy while minimizing side effects. Moreover, the development of novel imaging techniques, such as photoacoustic imaging and hybrid imaging systems, has further expanded the potential applications of molecular (nano)probes. By leveraging the unique properties of NPs, researchers are uncovering new methods to visualize cellular and molecular interactions *in vivo*, providing insights into disease mechanisms and treatment responses (Fig. 1). These innovations are particularly crucial in personalized medicine, where tailored diagnostic approaches can lead to more effective and precise therapies. Despite the promising advancements, challenges remain in the clinical translation of molecular imaging (nano)probes. Issues related to off-target effects, potential toxicity, and regulatory hurdles must be carefully addressed to ensure safety and efficacy in human applications.[25,27,28]

The purpose of this review is to provide a comprehensive overview of the latest developments in the field of molecular imaging, highlighting the transformative role of nanotechnology in enhancing diagnostic accuracy and specificity. By evaluating various types of molecular imaging (nano)probes, including fluorescence, photoacoustic, PET, MRI, and CT agents, we aim to elucidate the innovative strategies employed to target specific biological markers and processes, thereby improving disease detection, monitoring, and treatment response evaluation. Furthermore, the review seeks to address the challenges associated with the clinical implementation of these advanced molecular imaging techniques, such as biocompatibility/biosafety concerns, clinical translation studies, regulatory hurdles, and technical limitations, while also exploring future perspectives and potential directions for research and development.

2 Molecular imaging (nano)probes in medicine

Recent advancements in medical research and innovative chemical techniques have significantly accelerated the evolution and development of novel imaging (nano)probes,[4] which are described with more details in the following sections:

2.1. Magnetic resonance imaging (MRI) molecular probes

MRI is a fundamental tool in modern medical diagnostics and biomedical research due to its ability to provide high-resolution, non-invasive imaging of tissues and organs. Unlike other imaging techniques, MRI leverages the resonance of water protons or other nuclei to produce detailed anatomical and functional images. Its versatility in capturing signals from various nuclei with nuclear magnetic resonance (NMR) properties enables the study of a wide range of biological processes at molecular and cellular levels. This makes MRI one of the most significant tools for molecular imaging, particularly in tracking physiological and pathological changes in real-time.[29]

A critical advancement in MRI lies in the development of molecular imaging probes, which enhance the specificity and sensitivity of imaging. These probes are engineered to respond to specific biological or environmental stimuli, offering

valuable insights into functional and structural changes within tissues.[29,30] Recent years have witnessed a surge in the development of bio-responsive MRI probes capable of adapting their properties in response to fluctuations in local conditions, such as ion concentrations, pH, redox states, or enzyme activity. These probes are indispensable in functional imaging, bridging the gap between anatomical visualization and molecular diagnostics.[31–33] The functionality of MRI molecular probes is closely tied to advances in MRI methodologies, including the use of high magnetic fields and innovative techniques like chemical exchange saturation transfer (CEST) and hyperpolarized MRI. These approaches have expanded the capabilities of MRI in both clinical and research settings, allowing for a broader scope of applications.[34] For instance, bioresponsive MRI probes can detect dynamic changes in pH levels, metal ion concentrations, or enzymatic activity, contributing significantly to the understanding of physiological and pathological processes.[30] So far, several types of MRI probes have been introduced which are described in the follows.

2.1.1 Gadolinium-based MRI agent. Gadolinium-based MRI agents are widely used as contrast enhancers to improve the visibility of internal body structures during magnetic resonance imaging. Due to their paramagnetic properties, gadolinium compounds shorten the relaxation times of nearby water protons, resulting in clearer and more detailed MRI images.[35] To detect fibrin deposits in neuroinflammatory disorders a novel molecular imaging probe, EP2104-R (a short cyclic peptide stabilized by a disulfide bridge and conjugated to four Gd-DOTA chelates), was developed and its effectiveness was compared with a non-targeted gadolinium-based MRI agent, gadobutrol. Results of this study demonstrated that EP2104-R provided significantly higher contrast enhancement in T1-weighted MRI scans, allowing for clearer visualization of fibrin deposits, which are indicative of inflammation and blood–brain barrier disruption in MS. The enhanced contrast was most prominent in areas such as the meninges and perivascular spaces, key sites of fibrin accumulation during neuroinflammation. In comparison to the non-targeted gadolinium agent, EP2104-R showed markedly higher relaxivity (r_1), which refers to the efficiency of a contrast agent in enhancing signal intensity per unit concentration, with units of $mM^{-1}\ s^{-1}$. This contributed to the superior MRI signal in T1-weighted images. This enhancement provided more detailed and precise imaging of fibrin-rich regions, confirming the superior performance of the probe in neuroinflammatory imaging. *In vitro* studies further validated the specificity of EP2104-R by showing its strong and selective binding to fibrin, as opposed to fibrinogen, the precursor protein. Competitive binding experiments using EP2104-La, a non-paramagnetic analogue, inhibited the binding of EP2104-R to fibrin, reinforcing the probe's targeted action. EP2104-R was applied to a mouse model of experimental autoimmune encephalomyelitis (EAE), a model of MS, which led to high-resolution T1-weighted MRI of fibrin deposits in inflamed tissue. The intensity of the MRI signal strongly correlated with the severity of inflammation, as assessed through histological analysis, which revealed immune cell infiltration and demyelination in the affected regions. This association between fibrin deposition and disease severity underscores the potential of EP2104-R to monitor disease progression and treatment responses in real-time (Fig. 2).[36] Utilizing the T1-weighted imaging not only enabled accurate visualization of fibrin deposits, but also helped in tracking the progression of inflammation. The mentioned approach could have broad applications in early diagnosis, monitoring treatment efficacy, and understanding disease mechanisms in MS, as well as other neuroinflammatory conditions, such as Alzheimer's disease and traumatic brain injury.

Endothelial tight junctions maintained the structural integrity of blood vessels by controlling permeability between endothelial cells and regulating the movement of substances between the bloodstream and the inner layers of the aorta. Dysfunction of these junctions significantly contributed to the development of thoracic aortic aneurysm and dissection (TAAD). Their breakdown increased vascular permeability, allowing inflammatory cells such as neutrophils and macrophages to infiltrate the aortic wall. This infiltration triggered further inflammation and matrix degradation, resulting in aortic dilation and an elevated risk of dissection. The loss of tight junction integrity initiated a cascade of pathological events that accelerated aneurysm progression. To monitor these pathological changes, MRI was used due to its non-invasive nature and high-resolution capabilities. To improve the detection of endothelial dysfunction and vascular permeability, two gadolinium-based contrast agents, FITC-dextran-DOTA-Gd (fluorescein isothiocyanate-dextran conjugated with Gd-DOTA) and rhodamine B-dextran-DOTA-Gd, were synthesized using Gd-DOTA as the chelating unit. These agents were engineered to accumulate in aortic regions where endothelial tight junctions were compromised. The Gd-DOTA chelate enabled strong MRI signal enhancement, while the dextran component increased molecular size, promoting retention at sites of increased vascular permeability. MRI results showed that both FITC-dextran-DOTA-Gd and rhodamine B-dextran-DOTA-Gd accumulated in the thoracic aortas of BAPN-fed mice, a model for TAAD. This accumulation directly reflected endothelial barrier dysfunction, as the larger probes could permeate areas where tight junctions were disrupted. Enhanced contrast uptake was especially evident in regions with pronounced aortic dilation and dissection, corresponding to sites of severe tight junction impairment. These findings demonstrated that Gd-DOTA-based MRI contrast agents provided an effective and non-invasive method for visualizing endothelial dysfunction and tracking the progression of TAAD in real time.[37]

Peptide-functionalized liposomes were explored for their potential in targeted tumor imaging and therapy, with a specific focus on human carbonic anhydrase IX (hCAIX), a tumor-associated antigen commonly overexpressed in several cancers, including renal carcinoma. The approach aimed to enhance MR imaging and drug delivery using peptides with high affinity for hCAIX. Liposomes were functionalized with hCAIX-targeting peptides to enable selective binding to tumor cells. *In vitro* experiments using hCAIX-expressing cells confirmed strong and specific binding of the functionalized liposomes, demonstrated by increased fluorescence and MRI

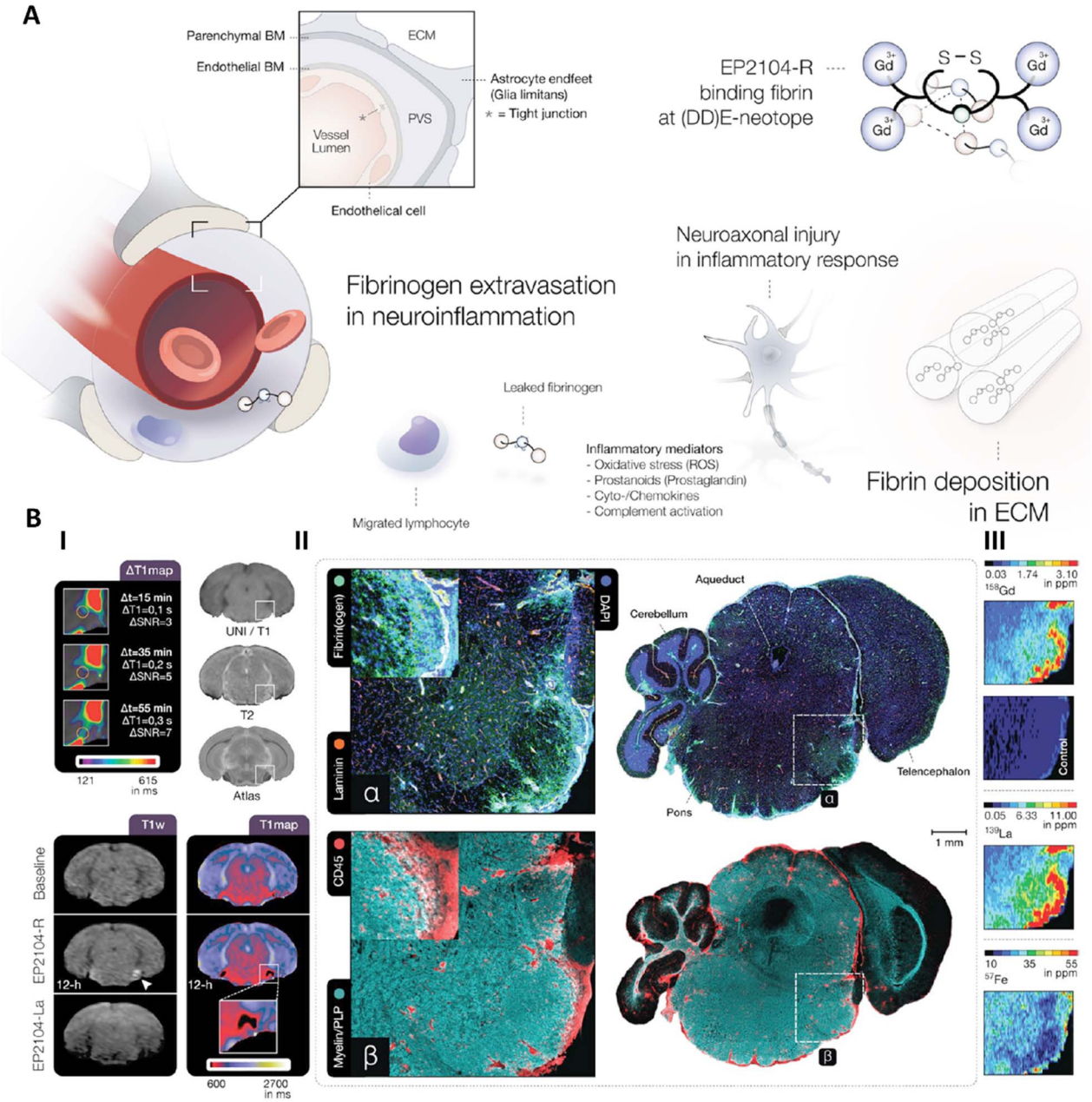

Fig. 2 (A) Fibrinogen extravasation in neuroinflammation. (B) (I) Displays a representative pontine EAE lesion with extended Gd uptake. Over 12 hours post-EP2104-R administration, fibrin-specific contrast enhancement (white arrow) remains visible but is displaced upon administering EP2104-La at a tenfold higher dose due to competitive binding. (II) Representative correlated immunofluorescence and confocal microscopy (IF-CM) images showing extensive fibrin(ogen) deposits (α) in the brainstem, which co-localize with CD45-positive immune cell infiltrates and mild demyelination (β). (III) describes LA-ICP-MS (Laser Ablation-Inductively Coupled Plasma Mass Spectrometry) analysis. Reproduced from ref. 36 under the terms of the Creative Commons (CC BY) license. Springer Nature, copyright 2022.

signal intensities compared to non-functionalized controls. Peptide modification significantly enhanced liposome–tumor interaction, promoting greater accumulation at the tumor site, which is essential for efficient targeted delivery. *In vivo* MRI results indicated that hCAIX-targeted liposomes yielded notably enhanced imaging contrast, attributed to the incorporation of the paramagnetic Gd-HPDO3A (gadolinium(III) 1,4,7-tris(carboxymethyl)-10-(2-hydroxypropyl)-1,4,7,10-tetraazacyclododecane) complex within the liposomal structure. This contrast agent increased MRI signal intensity at tumor regions, enabling high-resolution imaging, while, non-targeted liposomes showed reduced tumor accumulation and weaker MRI contrast. Beyond imaging applications, the peptide-functionalized liposomes also served as effective drug carriers. By targeting hCAIX-expressing tumors, they enabled site-specific delivery of chemotherapeutic agents, thereby reducing systemic toxicity and enhancing treatment precision. When loaded with anticancer drugs, the targeted liposomes achieved

greater drug accumulation in tumors and improved therapeutic efficacy. *In vivo* results demonstrated significantly greater tumor regression following treatment with targeted liposomes compared to non-targeted counterparts, confirming the value of this strategy in advancing cancer therapy.[38]

A comprehensive study introduced a novel imaging approach for detecting fibrosis in chronic kidney disease (CKD) using a targeted gadolinium-based MRI probe, Gd-OA. This probe was synthesized by functionalizing a gadolinium contrast agent with an oxoamide (OA) moiety, which selectively binds to allysine residues formed during collagen crosslinking, an early marker of fibrosis. By targeting collagen deposits, Gd-OA aimed to enhance MRI sensitivity for detecting kidney fibrosis, especially at early stages. The probe was tested in two fibrotic animal models: nephrotoxic nephritis (NTN) and Alport syndrome. Upon administration, Gd-OA significantly increased MRI signal intensity in fibrotic kidney regions, particularly in the cortex of NTN mice. This enhancement was attributed to the probe's specific binding to collagen fibers. A strong correlation (r^2 = 0.83) was observed between MRI signal changes (ΔR1) and hydroxyproline levels, a biochemical marker of fibrosis, confirming the probe's reliability. Comparative analysis with a non-targeted agent (Eu-DOTA) demonstrated that Gd-OA produced a much stronger signal, indicating its specificity for fibrotic tissue rather than nonspecific accumulation. Importantly, Gd-OA enabled the detection of early-stage fibrosis before noticeable kidney damage or functional decline, as serum creatinine and BUN levels remained stable—highlighting its potential for early diagnosis and therapeutic monitoring.[39] This study presents a promising advancement in the non-invasive imaging of fibrosis. The Gd-OA probe offered a high level of specificity and sensitivity for detecting kidney fibrosis at early stages, which could greatly enhance the ability to diagnose CKD sooner and track the effectiveness of anti-fibrotic treatments. This approach demonstrates strong potential for clinical application, particularly in scenarios requiring timely intervention to prevent irreversible renal damage.

2,2,6,6-Tetramethylpiperidinyloxy (TEMPO) radical dendrimers of generation 2 (G2) and a modified version with a 1,8-naphthalimide core (G2Naft) were synthesized to explore their potential as bimodal imaging agents for MRI and FI. The primary distinction between the two structures was the integration of the naphthalimide fluorophore in G2Naft, which imparted fluorescent capabilities in addition to the magnetic properties shared by both dendrimers. To ensure aqueous solubility both dendrimers were functionalized with amino acid salts. T1-weighted MRI scans performed in water showed that increasing the concentrations of TEMPO radicals led to brighter images, indicating enhanced contrast. Relaxivity measurements (r_1) revealed that G2 exhibited slightly higher relaxivity (1.5 $mM^{-1}\ s^{-1}$) compared to G2Naft (1.3 $mM^{-1}\ s^{-1}$), suggesting that the inclusion of the naphthalimide core could moderately reduce MRI contrast. Nevertheless, both dendrimers demonstrated r_1 values within the effective range of Gd^{3+}-based contrast agents. Moreover, the relaxivity values of G2 (0.18 $mM^{-1}\ s^{-1}$) and G2Naft (0.16 $mM^{-1}\ s^{-1}$) were comparable to that of free TEMPO, supporting their suitability as MRI contrast agents. Molecular dynamics (MD) simulations revealed structural differences between the dendrimers, G2 adopted a more compact, spherical conformation, whereas G2Naft initially formed a more extended structure before transitioning to a compact shape. G2 displayed stronger radical–radical interactions, with shorter inter-TEMPO distances, contributing to a slower rotational correlation time relative to G2Naft. These structural differences were consistent with the observed variation in MRI relaxivity. Simulations also suggested that the proximity of TEMPO units to the hydrophobic naphthalimide core in G2Naft could promote fluorescence quenching *via* photoinduced electron transfer (PET), which was supported by experimental fluorescence data. Despite partial quenching, G2Naft retained notable fluorescence properties in live mesenchymal stem cells (MSCs). The dendrimer efficiently internalized into cells, selectively staining the cytoplasm without affecting nuclei, indicating its potential for live-cell imaging. Furthermore, dual imaging functionality was achieved without compromising cellular viability or structural integrity.[40]

2.1.2 SPION-based MRI agent. A dual-modality imaging probe based on ultrasmall iron oxide NPs (Fe_3O_4–Cy) was developed to enable MRI-based monitoring of atherosclerotic plaque progression. This strategy was used to enhance the visualization of vascular morphology and plaque dynamics in a mouse model of atherosclerosis. T1-weighted MR imaging was performed following intravenous administration of Fe_3O_4–Cy at a dose of 0.1 mmol kg^{-1}. A notable increase in MRI signal intensity at plaque sites was observed over time, with significant enhancement detected as early as 0.5 hours post-injection. The signal continued to intensify, peaking at 72 h, indicating sustained NP accumulation within the plaques and providing a dynamic assessment of plaque development. The contrast-to-noise ratio (CNR) at the plaque regions significantly improved after nanoprobe injection, demonstrating the ability of probe to specifically localize to areas of plaque formation and enhance imaging clarity. Histological analysis confirmed the presence of iron oxide NPs within the plaque regions, validating the targeted accumulation of the probe. These findings highlighted the effectiveness of Fe_3O_4–Cy in delivering high-resolution, dynamic imaging of atherosclerotic plaques, making it suitable for long-term disease monitoring and early detection of cardiovascular abnormalities. The results also emphasized the potential of iron oxide NPs as efficient MRI contrast agents with excellent biocompatibility. Their sustained imaging performance and noninvasive functionality supported their clinical relevance, offering detailed insights into plaque structure and progression. This work provided a strong foundation for clinical translation by demonstrating both safety and efficacy, establishing Fe_3O_4–Cy as a promising tool for diagnostic imaging in atherosclerosis and related vascular conditions.[41] In this study, the use of ultrasmall Fe_3O_4–Cy NPs presents an exciting opportunity for advancing non-invasive imaging of atherosclerotic plaques. These dual-modality probes, with their ability to enhance T1-weighted MRI signals and specifically targeting plaque sites, offered significant potential for dynamic monitoring of plaque progression and morphology. Their biocompatibility and sustained imaging capabilities make them

a strong candidate for early detection and long-term management of cardiovascular diseases in clinical practice.

A dual-modality imaging probe was developed for the detection of atherosclerotic plaques, specifically targeting CD40, a cell surface receptor that belongs to the tumor necrosis factor receptor superfamily. The probe consisted of superparamagnetic iron oxide NPs (SPIONs) conjugated with Cy5.5, a near-infrared fluorescence dye. The primary aim of this work was to create a multimodal imaging agent capable of both MRI and optical imaging, offering enhanced sensitivity and specificity for detecting vulnerable plaques that are prone to rupture and can lead to acute coronary syndrome. The resulting probe, CD40-Cy5.5-SPIONs, was constructed by attaching a CD40 monoclonal antibody to the surface of SPIONs, followed by conjugation with Cy5.5 for FI. *In vitro* experiments demonstrated that CD40-Cy5.5-SPIONs specifically bound to tumor necrosis factor (TNF)-α-treated RAW 264.7 macrophages and MOVAS smooth muscle cells, confirming the probe's targeting ability. Confocal fluorescence microscopy and Prussian blue staining validated the successful binding of the NPs to these cells, indicating their potential for targeted imaging in atherosclerosis. *In vivo* studies were conducted in ApoE−/− mice fed a high-fat diet to induce atherosclerosis. Following intravenous injection of the probe, both FI and MRI were performed after 24 h. The FI results showed significantly stronger fluorescence signals in the atherosclerotic mice injected with CD40-Cy5.5-SPIONs compared to control groups. Additionally, T2-weighted MRI revealed marked contrast enhancement in the carotid arteries, supporting the potential of this probe for non-invasive detection of vulnerable plaques. This study suggested that CD40-Cy5.5-SPIONs offer a promising approach for multimodal imaging of atherosclerosis, with the ability to specifically target vulnerable plaques in both pre-clinical models and potentially in clinical settings (Fig. 3). Therefore, it could contribute in the growing field of molecular imaging, where the combination of MRI and optical imaging can provide enhanced diagnostic capabilities for cardiovascular diseases.[42]

MRI molecular probes enhance the specificity and sensitivity of imaging, enabling functional and anatomical insights into diseases. Advances like bio-responsive probes that detect changes in pH, enzymatic activity, or ion concentrations provide valuable data for understanding disease mechanisms. For example, fibrin-targeted MRI probes, such as EP2104-R, offer superior contrast for imaging neuroinflammation, outperforming traditional gadolinium-based agents in tracking blood–brain barrier disruptions. These developments underscore the importance of MRI probes in bridging the gap between molecular diagnostics and real-time monitoring.

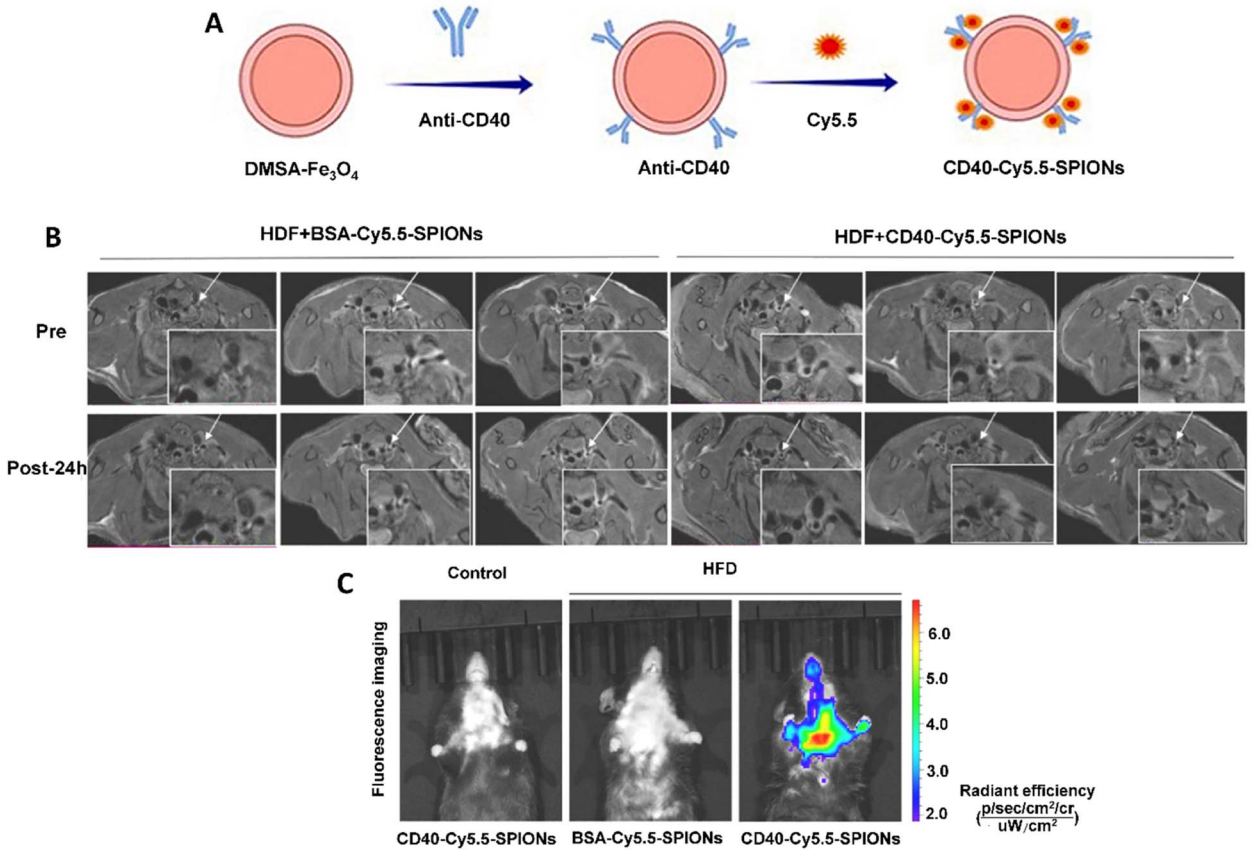

Fig. 3 (A) Scheme of synthesizing of CD40-Cy5.5–PIONs (B) *in vivo* T2-weighted MRI images of HFD-fed mice were taken both before and 24 hours after the injection of CD40-Cy5.5-SPIONs and BSA-Cy5.5-SPIONs, respectively. (C) *In vitro* fluorescence images. Reproduced from ref. 42 with permission from Elsevier B.V, copyright 2023.

2.2. Positron emission tomography (PET) molecular probes

PET is a non-invasive imaging technique that provides detailed, real-time insights into the molecular and cellular processes within the body by detecting the radiation emitted from positron-emitting radionuclides, which are typically attached to biologically active molecules, such as peptides, antibodies, or small molecules. These radionuclides decay and release positrons, which interact with electrons in the surrounding tissue, leading to the emission of gamma rays. The PET scanner detects these gamma rays and creates three-dimensional images that reveal the distribution and concentration of the radioactive tracer within the body.[43] This ability to visualize biochemical and metabolic activities makes PET an invaluable tool in the early diagnosis, staging, and monitoring of various diseases, particularly cancer, where it helps to identify tumors, assess their size, and monitor treatment response.[44] Moreover, the capacity of PET to provide both anatomical and functional information enhances its clinical applicability, offering a comprehensive approach to disease diagnosis and management. As the field continues to evolve, advancements in radiotracer development, including peptide-based probes, are pushing the boundaries of PET's diagnostic capabilities.[43,45]

In recent advancements in PET imaging, molecular probes, particularly those based on peptide ligands, have emerged as a highly promising class of agents due to their high target specificity, rapid clearance, and small molecular size, which allow for precise localization and minimal background interference. Peptidic PET probes offer several key advantages over traditional antibody-based agents, particularly in targeting small receptor sites or enzyme pockets, making them ideal for a wide range of targets such as cell surface receptors, transporters, and enzymes. These probes are often derived from natural products, such as peptides from proteins or intrinsic fragments; however, recent innovations have expanded this pool to include synthetic peptides, as well.[46] High-throughput peptide screening technologies, including mRNA and phage display methods, have played a pivotal role in identifying novel peptide sequences with enhanced binding affinity and specificity. These technologies allow for the rapid selection of peptides that bind tightly to their targets, while also minimizing non-specific interactions, which are crucial for improving the accuracy of PET imaging.[47] Moreover, the incorporation of macrocyclic structures and non-natural amino acids into peptide sequences has greatly improved the metabolic stability, pharmacokinetics, and target affinity of these probes, which is essential for maintaining their effectiveness *in vivo*.[18] These modifications ensure that the peptides remain intact long enough in the bloodstream to reach their intended target, while also enhancing their ability to cross biological barriers and bind to tumor sites or other diseased tissues with high specificity. As a result, peptide-based PET probes have gained substantial traction in clinical settings, particularly in oncology, where they are used to image various types of tumors such as neuroendocrine tumors, breast cancer, and gliomas.[46]

Labeling of peptides with radionuclides such as gallium-68 (^{68}Ga), fluorine-18 (^{18}F), and copper-64 (^{64}Cu) is a critical aspect of their effectiveness in PET imaging. The chelation of these radionuclides to the peptide is typically accomplished using well-established chelators like DOTA (1,4,7,10-tetraazacyclododecane-1,4,7,10-tetraacetic acid), NOTA (1,4,7-triazacyclononane-1,4-diacetic acid), or other bio-orthogonal conjugation methods like click chemistry. Among the most widely used, ^{68}Ga-labeled peptides have demonstrated excellent clinical success, particularly in the imaging of neuroendocrine tumors. Examples include [^{68}Ga]Ga-DOTA-TOC (octreotide), [^{68}Ga]Ga-DOTA-TATE (octreotate), and [^{68}Ga]Ga-DOTA-NOC, all of which target somatostatin receptors and have shown substantial diagnostic potential in PET imaging of neuroendocrine tumors. These agents provide high contrast and resolution images, enabling early detection and better assessment of tumor progression.[48]

In addition to ^{68}Ga-labeled peptides, more recent advancements have focused on improving the resolution and pharmacokinetics of peptide-based PET imaging agents through ^{18}F labeling. [^{18}F]AlF (aluminum-fluoride) chelation methods was developed to provide high-affinity, stable radiolabeling with favorable imaging properties. The development of these new fluorine-18-based methods aimed to improve the spatial resolution of PET imaging and shorten imaging acquisition times, making these agents more efficient for clinical applications. Additionally, fluorine-18-based radiotracers offer advantages in terms of longer half-life, which enables a greater reach in clinical applications across various patient populations.[49]

These advancements in peptide-based PET imaging agents are expanding their utility in various diagnostic fields, particularly in oncology, but also in the imaging of other diseases such as Alzheimer's and cardiovascular diseases.[50] The ability to use these probes to precisely map tumor locations and monitor therapeutic response in real-time has made peptide-based PET imaging a crucial tool in personalized medicine. With ongoing innovations in peptide design, labeling techniques, and targeted delivery strategies, the future of peptide-based PET imaging looks increasingly promising, offering more sensitive, specific, and clinically useful diagnostic agents for a wide range of diseases.[51,52]

2.2.1 Monomodal probes. Granzyme B (GZMB) was evaluated as a novel biomarker for inflammatory bowel disease (IBD) through the development of a radiolabeled imaging probe, ^{68}Ga-NOTA-GZP, designed for non-invasive detection of GZMB expression. The probe was synthesized by conjugating a GZMB-binding peptide (GZP) to the NOTA chelator and labeling the construct with gallium-68. Radiolabeling achieved an efficiency of 67% ± 11%, with radiochemical purity exceeding 95%. The probe maintained its radiochemical integrity under physiological conditions, demonstrating stability essential for *in vivo* imaging applications. Transcriptomic analysis across multiple datasets revealed consistent upregulation of GZMB in ulcerative colitis (UC) and Crohn's disease (CD), which was corroborated by immunofluorescence staining. GZMB was predominantly localized to the lamina propria of active IBD tissue, while its expression remained low in quiescent and healthy intestinal samples, confirming its role as a biomarker for active inflammation. The imaging performance of ^{68}Ga-NOTA-GZP was

assessed through biodistribution studies in mouse models, which showed rapid renal clearance and minimal non-specific tissue uptake, allowing for high-contrast PET imaging. The probe successfully visualized GZMB expression in inflamed intestinal regions. *In vivo* analysis using a dextran sulfate sodium (DSS)-induced colitis model in IL-10$^{-/-}$ mice showed significantly elevated probe uptake in inflamed intestines compared to healthy controls. Blocking experiments with unlabeled NOTA-GZP significantly reduced tracer uptake, confirming the probe's specificity for GZMB. Additionally, treatment with anti-TNF agents led to reduced PET signal, consistent with decreased inflammation as verified by histological and cytokine analyses. PET scans done over four weeks showed that the probe was taken up the most one week after colitis started, which matched the time when inflammation was at its highest. The signal slowly decreased as the inflammation reduce, and tests on colon tissues confirmed this by showing that the immune system was returning to normal after treatment. The probe displayed favorable biocompatibility, with minimal off-target effects and a distribution profile suitable for clinical translation. Overall, this PET imaging strategy enabled real-time, non-invasive monitoring of disease activity and therapeutic response in IBD, offering a valuable tool for patient management and evaluation of emerging treatments.[53]

CLDN18.2, a tight junction protein, was recognized as a critical biomarker due to its overexpression in several gastrointestinal cancers, making it highly suitable for targeted imaging and precision therapy. A PET imaging probe, [^{89}Zr]Zr-DFO-TST001, was developed to specifically detect and visualize the expression of CLDN18.2 in tumor tissues. The probe was constructed by radiolabeling the monoclonal antibody TST001, which possesses high affinity for CLDN18.2, with zirconium-89, using desferrioxamine (DFO) as the chelating agent to ensure stable and efficient radiolabeling. The synthesis began with conjugation of TST001 to DFO, a step validated to maintain the binding specificity of antibody toward CLDN18.2. The resulting radiolabeled probe exhibited excellent *in vitro* stability, retaining over 85% radiochemical purity under physiological conditions for up to 96 h, confirming its reliability as a PET imaging agent. *In vitro* studies demonstrated strong and selective binding to CLDN18.2, as significantly higher uptake was observed in CLDN18.2-positive BGC823CLDN18.2 cells compared to CLDN18.2-negative BGC823 cells. Blocking experiments using an excess of unlabeled TST001 antibody significantly reduced uptake in positive cells, further confirming the targeting specificity of probe. This selective binding was crucial for differentiating CLDN18.2-positive tumors from adjacent healthy tissues and achieving high imaging accuracy. A key strength of [^{89}Zr]Zr-DFO-TST001 was its compatibility with PET imaging, enabling high-resolution, non-invasive visualization of tumor sites. The probe effectively mapped CLDN18.2 expression, supporting its potential use in patient stratification and real-time monitoring of therapeutic response in gastrointestinal cancers. The use of biocompatible TST001 reduced the risk of immune-related side effects. Furthermore, application of zirconium-89 allowed for extended imaging timeframes, enhancing its suitability for *in vivo* applications. These features collectively underscored the clinical promise of [^{89}Zr]Zr-DFO-TST001 as a molecular imaging agent in targeted cancer diagnostics and treatment evaluation.[54]

Cluster determinant 30 (CD30) is a 120 kDa transmembrane glycoprotein and the eighth member of the tumor necrosis factor receptor superfamily (TNFRSF8). Due to its pivotal role in malignant lymphomas and elevated expression in some lung cancers, CD30 has been recognized as a promising diagnostic and therapeutic target. In a study, ^{89}Zr-labeled brentuximab vedotin (BV) was developed to enable *in vivo* tracking and PET imaging of CD30 expression in lung cancer zirconium-89. western blot analysis confirmed CD30 expression in three lung cancer cell lines (H460, H358, and A549), with H460 exhibiting the highest levels. Flow cytometry and saturation binding assays demonstrated strong binding affinity of both Df-BV and ^{89}Zr-Df-BV to CD30-expressing H460 cells. PET imaging and quantitative analysis revealed that ^{89}Zr-Df-BV showed the highest tumor uptake in H460 xenografts (9.93 $\pm$ 2.70% ID per g at 24 h post-injection), followed by H358 and A549 tumors. In contrast, ^{89}Zr-labeled nonspecific IgG exhibited low uptake in H460 models (5.2 $\pm$ 1.0% ID per g), confirming target specificity. Ex vivo biodistribution and immunohistochemistry supported the *in vivo* PET findings, and dosimetric extrapolation indicated a favorable safety profile. These results suggested that ^{89}Zr-Df-BV could serve as a valuable tool for noninvasive assessment of CD30 expression and biodistribution of brentuximab vedotin in lung cancer.[55]

A novel PET imaging probe was developed by radiolabeling IMMU-132, an FDA-approved antibody–drug conjugate (ADC) targeting Trop-2, with ^{124}I. Using a simplified *N*-chlorosuccinimide (NBS)-based one-step labeling method, they achieved over 99% radiochemical purity within one minute at room temperature, demonstrating a significant improvement over traditional labeling technique like ^{89}Zr. This efficient approach facilitated clinical translation and underscored the potential of ^{124}I for PET imaging applications. The PET imaging results demonstrated that ^{124}I-labeled IMMU-132 successfully targeted Trop-2-expressing tumors, providing precise, non-invasive visualization of Trop-2 expression and distribution *in vivo*. The probe allowed for real-time imaging of Trop-2-positive tumors, enabling early diagnosis and a deeper understanding of tumor biology. The high specificity and sensitivity of the radiolabeled IMMU-132 ensured that PET scans provided clear and detailed images, making it an effective tool for clinical use in identifying patients who could benefit from Trop-2-targeted therapies. Moreover, the study demonstrated the versatility of the ^{124}I-labeling approach for PET imaging. This method can be directly adapted to therapeutic radionuclides like ^{131}I and ^{177}Lu, allowing for a seamless transition from PET-based diagnosis to targeted radionuclide therapy. This theranostic potential positions ^{124}I-labeled IMMU-132 as a dual-functional probe capable of integrating imaging with treatment, significantly enhancing personalized cancer care. Compared to other Trop-2-targeted probes, such as nanobody-based agents, the IMMU-132-based PET probe exhibited superior binding affinity and therapeutic relevance. This dual-purpose design not only ensures effective PET imaging but also incorporates the cytotoxic drug SN-38,

enhancing its therapeutic value. These attributes positioned ^{124}I-labeled IMMU-132 as a first-in-class PET imaging agent for Trop-2-positive tumors, with applications in diagnosis, treatment planning, and efficacy monitoring.[56]

Multiple myeloma (MM) is a hematologic cancer marked by the proliferation of abnormal clonal plasma cells in the bone marrow and is the second most common blood malignancy. B-cell maturation antigen (BCMA), a member of the tumor necrosis factor receptor superfamily, is highly and selectively expressed on malignant plasma cells, playing a crucial role in MM progression. Due to its consistent and elevated expression, BCMA has emerged as an important biomarker for disease monitoring and a key target for immunotherapeutic approaches. Several BCMA-targeted therapies have been developed, including chimeric antigen receptor (CAR)-T cell therapy, bispecific T-cell engagers (BiTEs), and antibody–drug conjugates (ADCs) such as belantamab mafodotin. While these strategies have shown clinical efficacy, their long-term success depends on the stable and uniform presence of BCMA on tumor cells. Therefore, noninvasive methods for whole-body imaging of BCMA expression are valuable for guiding diagnosis, patient selection, and real-time evaluation of treatment response. In this context, a novel immunoPET probe, [^{89}Zr]Zr-DFO-PFBH0L0, was developed using a humanized anti-BCMA monoclonal antibody conjugated to deferoxamine (DFO) and labeled with zirconium-89. The resulting probe showed high *in vitro* stability and retained strong binding affinity toward BCMA-positive MM cells. *In vivo* PET imaging and biodistribution studies in mice models bearing H929 xenografts demonstrated selective and high tumor uptake (10.04 ± 1.04% ID per g), with a tumor-to-blood ratio exceeding 88, surpassing all control groups. Importantly, this study also reported the first BCMA-targeted PET/CT imaging in nonhuman primates (rhesus macaques), showing favorable pharmacokinetics, biodistribution, and metabolic stability, indicating strong translational potential. These findings established [^{89}Zr]Zr-DFO-PFBH0L0 as a promising immunoPET agent for the noninvasive, whole-body evaluation of BCMA expression in MM and related malignancies.[57]

2.2.2 Multimodal probes. A novel series of ^{68}Ga-labeled radiotracers was developed in a study for PET imaging targeting poly(ADP-ribose) polymerase-1 (PARP-1), an enzyme overexpressed in many tumor cells and involved in DNA repair. In here, Olaparib was structurally modified *via* replacing its cyclopropyl ring with DOTA for ^{68}Ga labeling and introducing alternative linkers to optimize pharmacokinetics. Three precursors—DOTA-Olaparib, DOTA-GABA-Olaparib, and DOTA-(Gly)3-Olaparib—were synthesized, characterized, and radiolabeled. These compounds showed high radiochemical purity (>97%), excellent stability in plasma, and high binding affinity to PARP-1 *in vitro*. Among the radiotracers, ^{68}Ga-DOTA-Olaparib demonstrated superior hydrophilicity, rapid clearance, and favorable biodistribution. PET/CT imaging in ovarian cancer-bearing mouse models revealed specific and high tumor accumulation of ^{68}Ga-DOTA-Olaparib, with tumor-to-muscle (T/M) ratios increasing over time. Biodistribution studies confirmed its selective tumor uptake and efficient renal excretion, reducing background signals in non-target abdominal tissues. Blocking experiments validated its specificity for PARP-1, while histological and immunohistochemical analyses corroborated these findings (Fig. 4).[58] We propose that ^{68}Ga-DOTA-Olaparib holds promise as a clinically translatable radiotracer for imaging PARP expression in ovarian cancer and detecting abdominal tumor metastases. In our opinion, optimizing tumor retention time and enhancing uptake, as compared to ^{18}F-labeled agents, could significantly improve its diagnostic performance.

A novel hybrid PET/MRI contrast agent, [^{18}F][Gd(FL^1)], was fabricated *via* combining gadolinium (Gd) and fluorine-18 (^{18}F) through a direct isotopic exchange. This agent was designed to retain the favorable properties of clinical gadolinium-based contrast agents (GBCAs), such as high relaxivity, excellent kinetic inertness, and rapid renal excretion, while also enabling reliable quantification through PET imaging. In terms of imaging, the dual-modality approaches provided significant insights into renal function. Biodistribution studies revealed that the fabricated agent was primarily concentrated in the urine and bladder, with substantial accumulation in the kidneys. The combination of PET and MRI proved to be highly effective in detecting abnormal renal filtration patterns. *In vivo* studies on healthy mice identified cases of unilateral retention of the agent, suggesting impaired renal function. MRI alone was less conclusive, particularly due to negative contrast effects, but PET imaging was able to quantitatively track the abnormal excretion of the agent, offering a precise method for detecting renal dysfunction. Moreover, the study demonstrated the advantage of combining PET and MRI. PET provided the ability to quantify renal excretion and distinguish abnormal filtration dynamics, while MRI offered anatomical details of kidney structures, providing critical spatial context. This dual-modality approach was especially valuable for assessing subtle renal dysfunctions, which might otherwise be missed with traditional imaging methods. The hybrid imaging system identified renal abnormalities that were not detectable with MRI alone, showcasing the synergistic potential of combining the two modalities.[59] Based on the findings from this study, the fabricated [^{18}F][Gd(FL^1)] hybrid contrast agent is an effective tool for detecting early-stage kidney disease, a condition that is challenging to diagnose with conventional imaging techniques. This approach, by offering both anatomical and functional insights, opens the way for further exploration into its application for other renal pathologies, setting the stage for future research into more precise diagnostic tools for renal diseases.

Gallium-68-labeled fibroblast activation protein inhibitor PET/CT (^{68}Ga-FAPI PET/CT) imaging was employed to assess the impact of combining transforming growth factor-beta receptor (TGF-βR) inhibition with immune checkpoint blockade (ICB) therapy in a mouse model of metastatic colorectal cancer (CRC). The primary goal of this study was to improve immunotherapy efficacy by targeting the tumor microenvironment (TME), particularly cancer-associated fibroblasts (CAFs), which contribute to immune evasion and therapeutic resistance. ^{68}Ga-FAPI PET/CT enabled non-invasive monitoring of CAF levels and provided dynamic, real-time visualization of TME

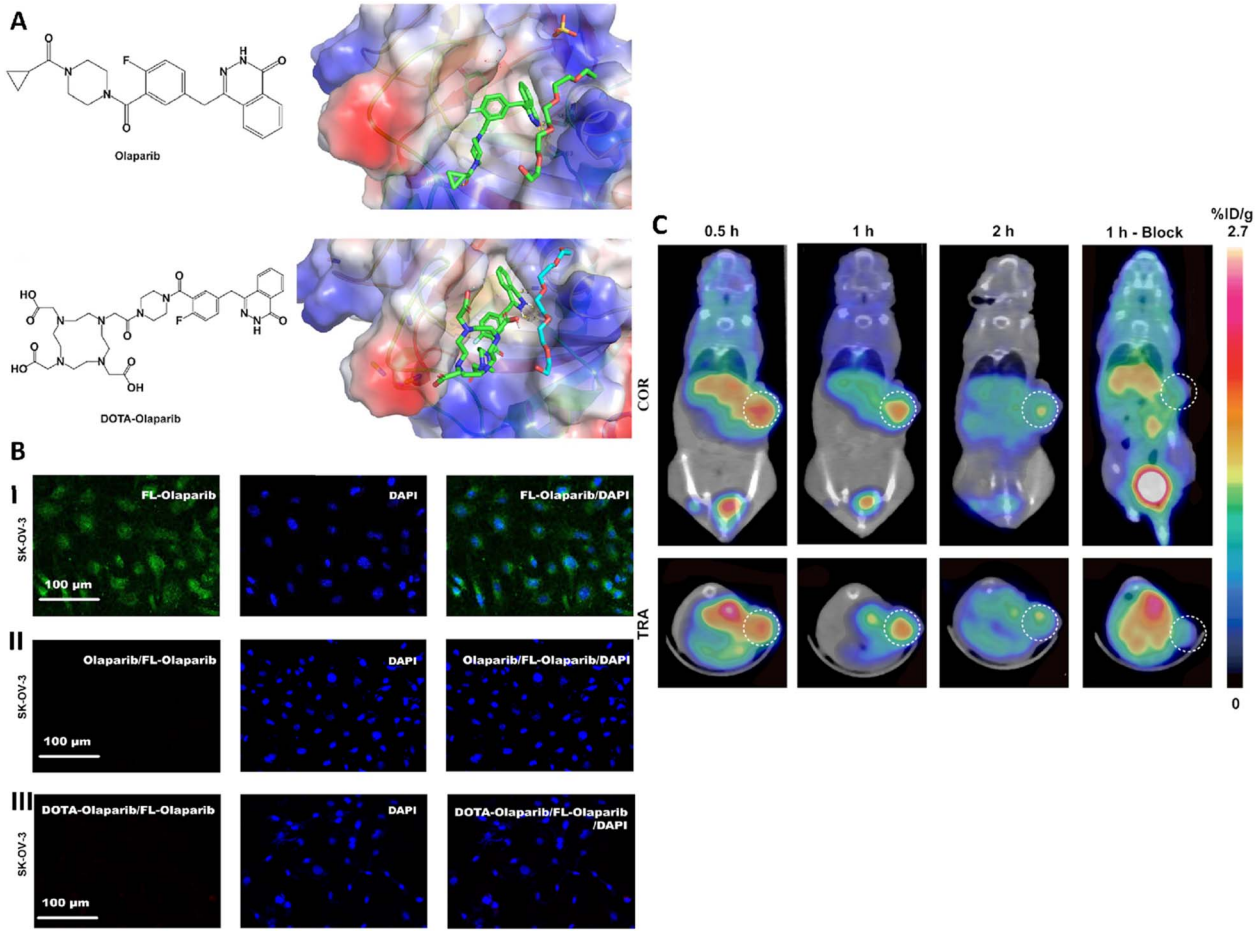

Fig. 4 (A) Design of ^{68}Ga-DOTA-Olaparib for PARP-1 binding, illustrating the structures of Olaparib and DOTA-Olaparib, their binding interactions with the PARP-1 catalytic domain, and molecular docking results. (B) (I) Confocal images of cells stained with FL-Olaparib (green) and DAPI (blue). (II) Confocal images of FL-Olaparib-stained cells with a 100-fold excess of Olaparib and DAPI. (III) Confocal images of FL-Olaparib-stained cells with a 1000-fold excess of DOTA-Olaparib and DAPI. (C) PET imaging of ^{68}Ga-DOTA-Olaparib in SK-OV-3 models at 0.5, 1, and 2 h post-administration using MicroPET/CT. Reproduced from ref. 58 under the terms of the Creative Commons CC BY license. Springer Nature, copyright 2023.

alterations. The imaging revealed a significant reduction in CAF density in tumors treated with the combination therapy, demonstrating the ability of TGF-βR inhibition to remodel the TME and enhance ICB response. The probe also facilitated tracking of tumor regression and metastatic spread. Treated mice exhibited significant reduction in tumor volume and liver metastases compared to controls, findings supported by histological analysis confirming reduced myofibroblastic and inflammatory CAF populations. Beyond CAF targeting, ^{68}Ga-FAPI PET/CT also allowed assessment of immune cell activity within tumors. The combination therapy promoted increased infiltration of CD^{8+} and CD^{4+} T cells, contributing to a more robust antitumor immune response. This immune activation was corroborated by PET/CT imaging, which provided spatial and quantitative insights into treatment efficacy. Overall, ^{68}Ga-FAPI PET/CT served as a valuable imaging platform for evaluating therapeutic response, TME remodeling, and immune activation in real-time, highlighting its potential in guiding and optimizing combination cancer therapies (Fig. 5).[60]

In a first-in-human phase 1 clinical trial study, the innovative PET radiotracer zirconium-89-desferrioxamine (^{89}Zr-Df-IAB22M2C) was developed to visualize CD^{8+} T-cell infiltration in solid tumors. This radiotracer provided a non-invasive means to evaluate immune activity within the tumor microenvironment. The trial involved patients with solid tumors, divided into dose-escalation and dose-expansion phases. The imaging protocol utilized PET/CT, which is a highly sensitive modality capable of detecting minute amounts of radiotracers and providing detailed spatial and functional data. PET imaging with ^{89}Zr-Df-IAB22M2C allowed the visualization of CD^{8+} T-cell distribution across normal tissues, immune organs, and tumor sites. The radiotracer showed favorable pharmacokinetics, with a biexponential clearance pattern, meaning the minibody cleared rapidly from the bloodstream at lower doses and displayed slower clearance at higher doses. Notably, at doses of 1.5 mg or lower, the minibody was undetectable in serum after 48 h, which minimized background signal and optimized image quality. Biodistribution analysis revealed the highest

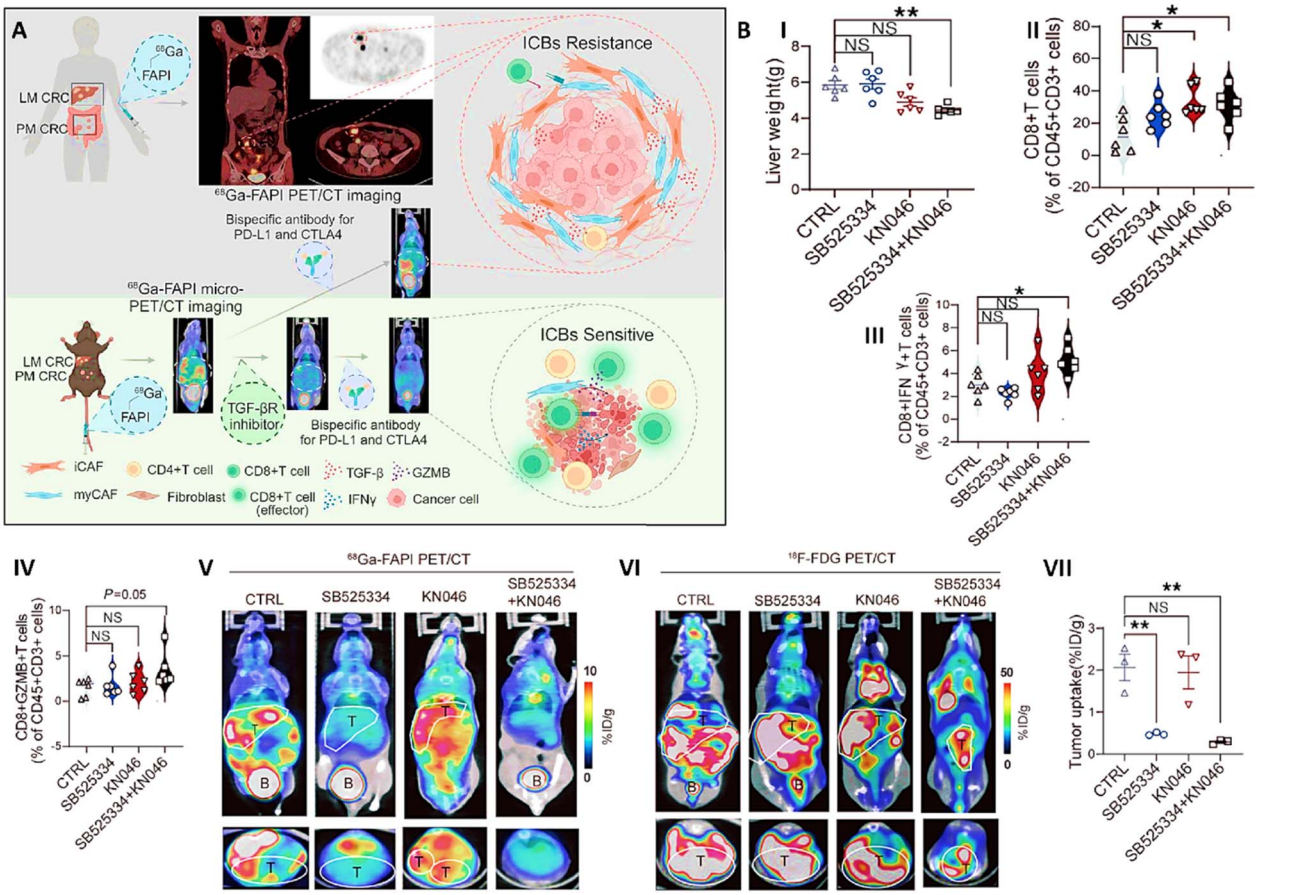

Fig. 5 (A) Schematic image related to the application of ^{68}Ga-FAPI-04 prob for PET/CT imaging of colorectal cancer. (B) Effect of different treatments (CTRL: control, SB525334: transforming growth factor-β receptor type 1 (TGF-βR) inhibitor, KN046: bispecific antibody used for blocking programmed death-ligand 1 (PD-L1) and cytotoxic T-lymphocyte-associated protein 4 (CTLA-4), and combination of SB525334 and KN046) on liver weights (I), CD^{8+} T cells (II), $CD^{8+}IFN\text{-}\gamma^{+}$ T cells (III), and $CD^{8+}GZMB^{+}$ T cells (IV) of mice had MC38 liver metastasis. ^{68}Ga-FAPI PET/CT (V) and ^{18}F-FDG PET/CT (VI) images of cancerous mice exposed with different treatments (T: tumor, B: bladder). (VII) Percentage of ^{68}Ga-FAPI tumor uptake in cancerous mice exposed with different treatments. Reproduced from ref. 60 under the terms of the Creative Commons Attribution 4.0 International License. American Society for Clinical Investigation (ASCI), copyright 2024.

radiotracer uptake in tissues rich in CD^{8+} T cells, such as the spleen, bone marrow, and liver. This aligns with the role of these organs in immune regulation and CD^{8+} T-cell activity. In contrast, minimal uptake was observed in CD^{8+}-poor tissues like muscle and lung, highlighting the specificity of ^{89}Zr-Df-IAB22M2C for CD^{8+} T-cell-rich environments. Tumor uptake of the radiotracer was evident in 67% of the lesions, with higher uptake observed in patients undergoing immunotherapy (88%). PET imaging successfully differentiated immune-active tumors from inactive ones, providing critical insights into the immune status of the tumor microenvironment. The results also emphasized the utility of ^{89}Zr-Df-IAB22M2C PET/CT in assessing immunotherapy responses. For instance, in one case, a melanoma patient with high CD^{8+} uptake on PET/CT showed a complete response to pembrolizumab, sustaining remission for over two years. Another patient with metastatic melanoma demonstrated tumor uptake consistent with stable disease, while a third case of hepatocellular carcinoma revealed increased CD^{8+} infiltration post-nivolumab treatment, corresponding to tumor progression on follow-up imaging. These case studies underscored the potential of ^{89}Zr-Df-IAB22M2C PET/CT as a powerful biomarker for immune activity and treatment monitoring.[61]

Immunotherapy has emerged as an effective cancer treatment, particularly through the use of immune checkpoint inhibitors (ICIs) targeting programmed cell death protein 1 (PD-1), programmed cell death ligand 1 (PD-L1), and cytotoxic T lymphocyte antigen 4 (CTLA-4). In clinical settings, PD-L1 expression is commonly assessed by immunohistochemistry (IHC) to guide treatment decisions. However, IHC results often vary due to differences in detection platforms, scoring criteria, and tumor heterogeneity. Since IHC provides only localized information from limited tissue samples, it fails to represent the full extent of PD-L1 expression. This heterogeneity contributes to inconsistent responses to ICIs, underscoring the need for sensitive and noninvasive imaging approaches. To address this, a dual-modality positron emission tomography/near-infrared fluorescence (PET/NIRF) imaging probe targeting PD-L1 was developed using an aptamer-based platform. The probe precursor, NOTA-Cy5-R1, was synthesized *via* automated solid-phase

oligonucleotide synthesis and subsequently radiolabeled with gallium-68 to yield [^{68}Ga]Ga-NOTA-Cy5-R1. *In vitro* assessments using flow cytometry, fluorescence imaging, and cellular uptake studies demonstrated that the probe bound specifically to PD-L1-expressing A375-hPD-L1 cells, exhibiting good stability and fluorescence properties. *In vivo* imaging confirmed that [^{68}Ga]Ga-NOTA-Cy5-R1 probe selectively accumulated in PD-L1-positive tumors while rapidly clearing from non-target tissues, resulting in high signal-to-noise ratios. In A375-hPD-L1 xenografts, strong fluorescence signals were detected over time, with a tumor-to-muscle (T/M) ratio over 2.5 at 2 hours post-injection. A375 tumors showed negligible signal, reinforcing the probe's PD-L1 specificity. Strong fluorescence in the kidneys indicated renal clearance of the probe. In NCI-H1299 xenografts, PET imaging with [^{68}Ga]Ga-NOTA-Cy5-R1 showed low uptake without treatment. Following cisplatin therapy, tumor uptake significantly increased after the second and third treatment rounds, indicating upregulated PD-L1 expression. Ex vivo autoradiography and western blot confirmed these findings, showing about a twofold increase in tracer accumulation and PD-L1 levels. These results demonstrated that the probe could sensitively monitor therapy-induced changes in PD-L1 expression. These imaging results were consistent with ex vivo autoradiography and western blot analyses. Overall, [^{68}Ga]Ga-NOTA-Cy5-R1 demonstrated strong potential as a dual-modality imaging agent for visualizing PD-L1 expression and tracking its dynamic changes, offering a promising tool for guiding and optimizing immune checkpoint inhibitor therapy in clinical practice.[62]

PET molecular probes provide unparalleled precision in visualizing molecular and cellular activities. Peptide-based probes like [^{68}Ga]Ga-DOTA-TATE for neuroendocrine tumors exemplify how PET imaging enables early diagnosis and therapeutic monitoring. Recent innovations, such as [^{68}Ga]-labeled FAPI tracers, have expanded PET applications to monitoring tumor microenvironments and fibroblast-associated diseases. By integrating advanced radiotracer designs, PET probes offer highly specific, non-invasive imaging solutions critical for personalized medicine and targeted therapies.

2.3. Computed tomography (CT) molecular probes

CT is widely used for non-invasive imaging due to its high resolution, speed, and broad clinical applications. Normally, iodinated contrast agents are used as contrast agents for CT imaging; however, they often require large concentrations and have rapid clearance from the body, limiting their use for molecular imaging. To overcome these limitations, researchers have turned to NPs as enhanced CT contrast agents. These NPs, such as those incorporating iodine, Au, and bismuth, exhibit high electron density, long circulation times, and preferential accumulation in tumors due to the enhanced permeability and retention (EPR) effect.[63]

2.3.1 Iodine labeled probes. One promising approach for enhancing CT molecular imaging is the development of iodinated nanoscale activity-based probes (IN-ABPs), which target specific biological markers to improve contrast sensitivity. IN-ABPs are designed to covalently bind to target proteases, such as cysteine cathepsins, that are overexpressed in cancers. These probes consist of a targeting peptide, an electrophilic "warhead" that facilitates covalent binding, and an iodine-based contrast agent. In a study exploring this concept, IN-ABPs with varying iodine contents (up to 48 iodine atoms) were developed to target cathepsins B, L, and S. These probes demonstrated increased tumor accumulation and enhanced CT contrast, with the 48-iodine-tagged version producing over 2.1 times higher signals compared to its nontargeted counterparts. The successful development of such probes highlights their potential for molecular imaging of cancers, providing both improved detection and targeted therapeutic opportunities.[64] This strategy of using high-density iodinated NPs linked to molecular targets represents a significant advancement in CT imaging, offering a way to overcome the sensitivity limitations of traditional CT contrast agents while enabling precise, molecular-level imaging of cancer.

A novel strategy was employed to improve the pharmacokinetics and imaging capabilities of FAPI-based tracers by incorporating a maleimide group into the FAPI-04 molecule, resulting in the formulation of DOTA-FAPI-maleimide. This structural modification enhanced the affinity of the probe for endogenous albumin, significantly prolonging its circulation time in the bloodstream. As a result, the tracer exhibited delayed clearance and increased tumor accumulation, leading to more efficient tumor targeting and improved retention within tumor tissues. The maleimide-functionalized probe demonstrated superior tumor-specific uptake, particularly in HT-1080-FAP xenografts, where accumulation was markedly higher than that of the conventional FAPI-04 tracer. When combined with CT imaging, the modified probe enabled high-contrast visualization of tumors, producing significantly improved tumor-to-background ratios. Contrast-enhanced CT scans revealed that the probe provided clearer and more detailed tumor imaging, with enhanced delineation of tumor margins due to its prolonged intratumoral retention. This advantage was especially evident in an ovarian cancer PDX model, where CT imaging showed increased tracer uptake and reduced background signal, resulting in sharper contrast and improved image clarity. The extended retention time further enhanced the effectiveness of late-phase imaging, offering deeper insight into internal tumor architecture. These enhancements proved critical for visualizing smaller or deep-seated tumors that may not be easily detected using conventional imaging techniques. CT imaging with the DOTA-FAPI-maleimide probe offered greater specificity and sensitivity compared to standard FAPI-based agents, facilitating more accurate tumor localization. The maleimide group contributed to prolonged tumor site retention, which benefited both early- and late-phase imaging, enabling high-resolution visualization of tumor boundaries. This capability is vital for precise diagnosis and may support targeted therapeutic interventions. Additionally, the *in vivo* stability and sustained performance of the modified probe suggested strong potential for clinical translation, particularly in applications requiring prolonged imaging for treatment monitoring and planning.[65]

A type of radiolabeled human serum albumin (HSA) was produced as a platform to enhance the detection of atherosclerosis (AS) plaques, particularly by targeting the folate receptor beta (FR-β). Multiple tracers were synthesized using both covalent and non-covalent radioiodination techniques, and folate molecules were successfully conjugated to HSA. Among the formulations, [^{131}I]HF exhibited notable stability in mouse serum, which was essential for preserving tracer integrity during imaging. *In vitro* assays demonstrated strong binding affinity of the radiotracers to folate-conjugated HSA (HSA-FA), with [^{131}I]IBA showing particularly high affinity. This interaction was further validated in macrophage cell models, which exhibited substantial uptake of the radiolabeled tracers. Initial biodistribution data indicated tracer accumulation in the blood and liver, followed by clearance from non-target tissues over time, which significantly reduced background signals and enhanced imaging clarity of AS plaques. Histological evaluation of aortic tissue from atherosclerotic mice confirmed elevated FR-β expression in plaque-associated activated macrophages, supporting its relevance as a biomarker for AS. Micro SPECT-CT imaging successfully visualized atherosclerotic lesions with high contrast and minimal signal interference from surrounding tissues. The approach provided a clear and sensitive imaging modality, making it a promising non-invasive strategy for detecting and assessing atherosclerotic plaque development (Fig. 6).[66]

2.3.2 Other types of labeled probes. Besides iodine, other types of labeling compounds were also used for producing probes used for enhancing CT imaging. For instance, in a study, the diagnostic utility of ^{68}Ga-FAPI PET/CT was assessed in patients with head and neck cancer of unknown primary (HNCUP) and compared to conventional ^{18}F-FDG PET/CT. The study focused on evaluating the effectiveness of ^{68}Ga-FAPI PET/CT in identifying primary tumors that remained undetectable

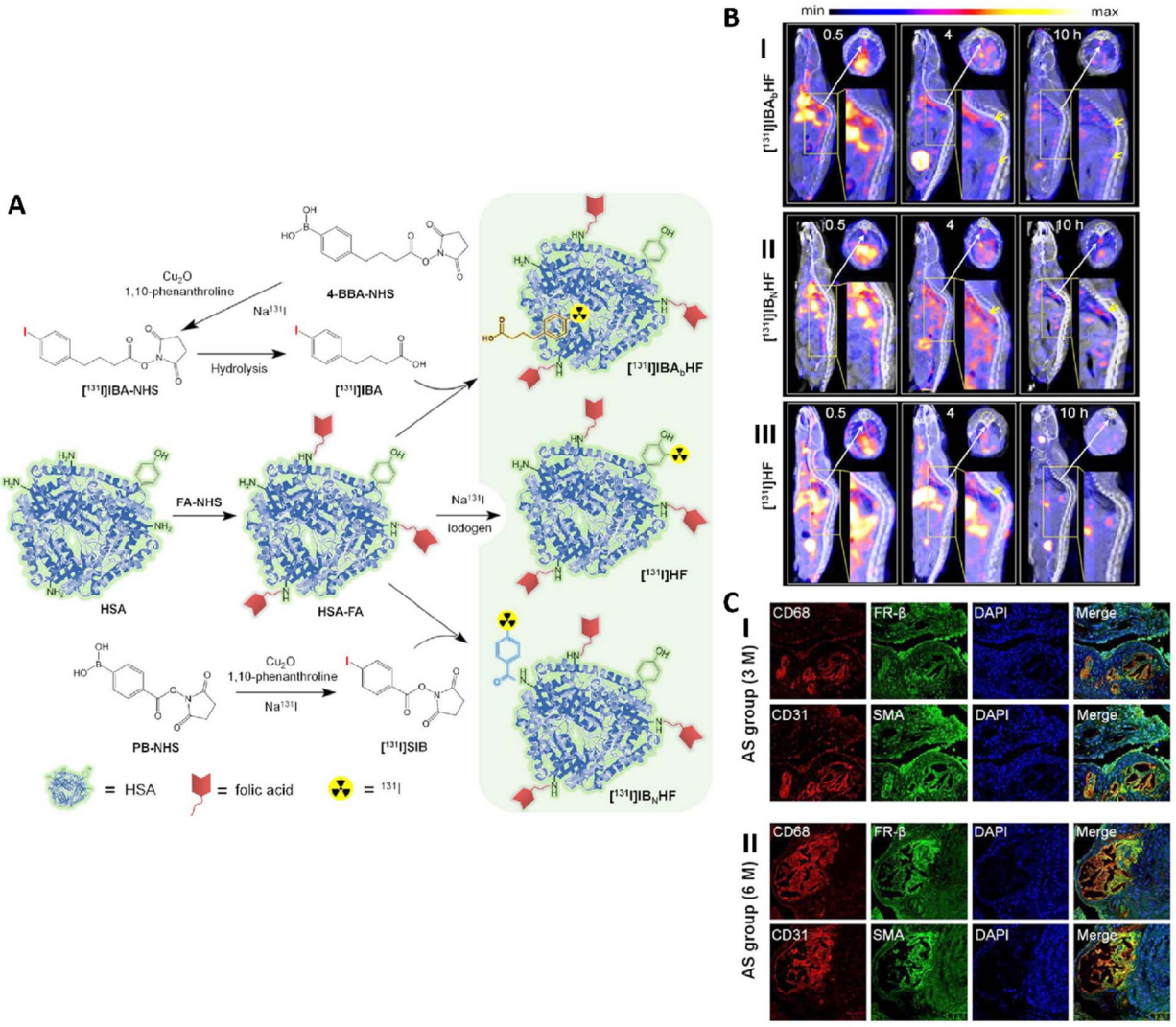

Fig. 6 (A) Preparation of [^{131}I]IBAbHF, [^{131}I]IBNHF, and [^{131}I]HF. (B) SPECT images (Ax and Sag) of [^{131}I]IBAbHF (I), [^{131}I]IBNHF (II), and [^{131}I]HF (III) in ApoE−/− AS groups (6 M) at 0.5, 4, and 10 h p.i. The lesions and nontarget regions were indicated by the yellow arrows and circles, respectively. (C) (I and II) Colocalization of FR-β (green) *vs.* CD68 (red) and α-SMA (green) *vs.* CD31 (red) within aortic sections of the WT and AS (3 and 6 M) mice. Reproduced from ref. 66 with permission from American Chemical Society, copyright 2023.

through standard diagnostic methods. Key performance metrics such as sensitivity, specificity, and diagnostic accuracy were analyzed to determine the comparative advantage of this imaging modality. Results demonstrated that ^{68}Ga-FAPI PET/CT showed better performance than ^{18}F-FDG PET/CT, particularly in detecting primary tumors located in the oropharyngeal region. The tracer showed higher sensitivity and a greater positive predictive value, enabling more precise identification of small oropharyngeal tumors that were often missed using ^{18}F-FDG PET/CT. Additionally, ^{68}Ga-FAPI PET/CT proved more effective in detecting metastatic lymph nodes, which is critical for accurate staging and treatment planning in HNCUP cases. The CT component further enhanced diagnostic accuracy by providing high-resolution anatomical detail, which allowed for precise localization of tumor sites and identification of structural abnormalities such as enlarged lymph nodes or tissue changes related to tumor growth. The integration of metabolic imaging *via* PET with anatomical data from CT offered a comprehensive view of tumor burden, spread, and proximity to adjacent tissues. Notably, ^{68}Ga-FAPI PET/CT revealed previously undetected primary tumors in several patients, leading to revised clinical staging and changes in treatment plans. This improved localization reduced the need for invasive procedures like diagnostic tonsillectomy, often employed when the tumor origin is unknown. By enhancing tumor detection and staging accuracy, ^{68}Ga-FAPI PET/CT contributed to more informed clinical decisions and showed potential for improving treatment outcomes and patient prognosis in HNCUP.[67]

A fibrin-targeting nuclear imaging probe, A16, based on α2-antiplasmin (α2-AP), was developed for the detection of thrombi, a critical issue in thrombotic disease diagnosis and treatment. The probe was conjugated with diethylenetriamine pentaacetic acid (DTPA) for labeling with indium-111 (^{111}In) and rhodamine B that enabled a comprehensive and highly sensitive method for thrombus detection. Results demonstrated that A16 exhibited significantly higher incorporation into human thrombi compared to previously developed fibrin-targeting probes, suggesting a more robust affinity for fibrin, a central component in thrombus formation. *In vitro* analysis showed that A16 exhibited strong binding to fibrinogen and fibrin, which was confirmed by using various thrombus models, including human thrombi and fibrin-embedded gels. The probe displayed an excellent ability to localize and accumulate in thrombotic regions, demonstrating superior performance to conventional thrombus imaging agents. Moreover, *in vivo* imaging using single-photon emission computed tomography/computed tomography (SPECT/CT) in mouse models allowed for precise and detailed visualization of thrombus formation. The high sensitivity of this probe enabled the detection of thrombi in both arterial and venous systems, even in smaller thrombus models, making it a promising candidate for early detection of thrombotic events. The SPECT/CT imaging revealed a clear contrast between thrombotic tissue and surrounding areas, indicating high specificity in targeting fibrin. Further evaluation of the probe's potential in clinical scenarios showed that A16 could be effectively used to assess the effectiveness of thrombolytic therapies. In treatment studies with a thrombolytic agent, a significant reduction in thrombus size was observed, which corresponded to a decrease in probe accumulation in the affected tissue. This demonstrated the ability of A16 to not only detected thrombus formation but also tracked the dynamic changes during treatment, making it a useful tool for monitoring the success of therapeutic interventions. Additionally, the probe showed minimal accumulation in non-target tissues, confirming its high specificity and low off-target effects.[68]

A comprehensive study was done to investigate the potential of molecular imaging for detecting thromboembolic diseases, specifically targeting factor XIIa (FXIIa), a critical enzyme in the coagulation pathway involved in thrombus formation. In here, a novel imaging probe was developed *via* conjugating a human monoclonal antibody, 3F7, which specifically binds to FXIIa, with a near-infrared (NIR) dye for use in molecular imaging. This probe was designed to selectively target thrombi, enabling the detection of thromboembolic diseases through fluorescence and CT imaging techniques. *In vitro* studies demonstrated that 3F7-NIR exhibited high binding affinity to thrombi, with significantly higher fluorescence intensity observed when compared to a control antibody. These results indicated that the probe selectively targeted thrombotic tissues, allowing for potential detection of thrombus presence with high specificity. Furthermore, the study expanded its focus to *in vivo* imaging, using a $FeCl_3$-induced carotid thrombosis model in mice. The results from this model were particularly compelling, as the 3F7-NIR probe successfully identified thrombus formations through both fluorescence and CT imaging. The fluorescence signals were localized to the thrombus, confirming the specificity and efficacy of the probe in detecting acute thrombi. The CT scans provided detailed imaging, revealing the precise location of thrombi in the carotid artery, with enhanced contrast between the thrombus and surrounding tissue, demonstrating the potential of combining molecular imaging with CT for accurate thrombus detection. The 3F7-NIR probe could bind to thrombi that suggest its potential for monitoring thrombus formation over time. This capability is crucial for the diagnosis and management of thromboembolic diseases, as it can help in assessing the age of thrombi and providing more accurate clinical information. In addition to the carotid thrombosis model, they tested the probe in a pulmonary embolism (PE) model in mice. The 3F7-NIR probe demonstrated effective targeting and imaging of thrombi in the lungs, where it showed strong fluorescence signals, confirming the versatility of this probe in detecting thromboembolic diseases beyond arterial thrombi. Moreover, CT imaging provided excellent contrast, enabling clear visualization of thrombus locations in the pulmonary vasculature. Overall, these results demonstrated the probe's ability to non-invasively detect thromboembolic diseases in both arterial and venous systems with high specificity and imaging clarity.[69]

A comprehensive study utilized [^{11}C]OMAR, a PET imaging probe targeting cannabinoid receptor type 1 (CB1R), to evaluate CB1R expression in bone and brain tissues of cynomolgus monkeys. The study included nine monkeys, four post-menopausal osteoporotic and five young healthy females,

whose bone density was assessed by Quantitative Computed Tomography (QCT) alongside serological tests. PET/CT imaging focused on CB1R expression in the lumbar spine and brain. QCT results showed a significant reduction in lumbar spine bone mineral density (BMD) in osteoporotic monkeys compared to healthy controls. PET/CT revealed markedly increased CB1R expression in the lumbar spine of osteoporotic animals, with elevated Standard Uptake Values (SUVs) indicating heightened receptor activity. Brain scans showed higher CB1R uptake in regions such as the thalamus and prefrontal cortex in osteoporotic monkeys, and this increase negatively correlated with lumbar BMD, suggesting a link between brain CB1R expression and bone density. Additionally, CT imaging demonstrated elevated CB1R uptake in the cervical spine of osteoporotic monkeys, reinforcing CB1R's potential involvement in osteoporotic bone disease.[70]

A targeted imaging probe was developed for liver cancer *via* employing PET/CT to enhance diagnostic precision. The focus of their study was glypican-3 (GPC3), a cell surface proteoglycan overexpressed in hepatocellular carcinoma (HCC). Two variants of a radiolabeled single-domain antibody specific to GPC3, ^{89}Zr-ssHN3 (site-specific conjugation) and ^{89}Zr-nHN3 (non-specific lysine-directed conjugation), was produced *via* utilizing a desferrioxamine (DFO) chelator for zirconium-89 labeling. The imaging results obtained from PET/CT revealed significant differences between two probes in terms of tumor specificity, biodistribution, and imaging clarity. ^{89}Zr-ssHN3 exhibited a marked improvement in tumor uptake, with nearly three-fold higher tumor-to-liver signal ratios compared to ^{89}Zr-nHN3. This was particularly important in the context of CT imaging, where anatomical contrast between tumor tissue and surrounding liver tissue is often challenging to discern. The high tumor-to-liver contrast provided by ^{89}Zr-ssHN3 allowed for more precise localization of GPC3-expressing tumors on PET/CT images, addressing a critical limitation in conventional imaging for liver cancer. Additionally, ^{89}Zr-ssHN3 showed superior pharmacokinetics with reduced off-target accumulation in non-tumor liver tissue and blood. This feature was crucial in the CT component of the PET/CT scans, as it minimized the background noise and enhanced the structural resolution of the liver and tumor margins. When compared to the widely used ^{18}F-FDG tracer, ^{89}Zr-ssHN3 offered enhanced tumor detection and significantly lower uptake in non-cancerous liver regions, making it a more effective imaging tool for HCC.[71]

CT molecular probes address the limitations of traditional iodinated agents by utilizing NP-based designs for improved contrast and longer retention at target sites. For example, iodinated nanoscale probes targeting cysteine cathepsins offer superior contrast sensitivity in tumor imaging. Maleimide-modified FAPI tracers further enhance tumor visualization by increasing retention in diseased tissues. These innovations exemplify how CT molecular probes improve diagnostic precision, making them indispensable for real-time monitoring and disease progression assessment.

2.4. Photoacoustic molecular imaging probes

PAI is a cutting-edge hybrid imaging modality that combines the high spatial resolution of ultrasound with the molecular sensitivity of optical imaging. This technique has emerged as a promising tool for *in vivo* molecular imaging due to its ability to provide both high-resolution images and deep tissue penetration. PAI relies on the photoacoustic effect, where tissue absorbs laser light (usually in the NIR spectrum) and then emits ultrasound waves that can be captured to generate detailed images of the tissue.[72] Molecular probes used in PAI are designed to absorb light in the NIR region, which allows them to penetrate into the deeper tissues with minimal scattering, enabling the visualization of structures at greater depths compared to conventional optical imaging techniques. These probes are often based on nanomaterials such as Au NPs, carbon nanotubes, organic dyes, and graphene oxide, which possess strong optical absorption properties in the NIR spectrum.[73,74] Additionally, the strong light-to-sound conversion efficiency of these nanomaterials makes them ideal candidates for PAI. The use of molecular probes in PAI is enhanced by functionalization with targeting ligands, such as antibodies, peptides, or aptamers, which enable specific binding to biomarkers expressed on the surface of diseased tissues, including tumors, inflammation, and other pathological conditions.[73,75] This targeted approach allows for the precise localization of the probe at the desired tissue, improving the sensitivity and specificity of the imaging technique. For example, some probes are engineered to target tumor-associated biomarkers, facilitating the detection of early-stage tumors or monitoring tumor progression in real-time.[73]

Recent advancements in PA molecular probes have focused on improving the targeting efficiency, biocompatibility, and imaging performance of these probes. For example, the incorporation of stimuli-responsive materials has enabled probes to release imaging agents in response to environmental changes, such as changes in pH, temperature, or the presence of specific enzymes, enhancing their effectiveness in specific pathological contexts.[76] Additionally, the development of NPs with enhanced photothermal properties has broadened the scope of PAI in therapeutic applications, such as in photothermal therapy, where the same probe can be used for both imaging and treatment.[77] In clinical and preclinical settings, PA molecular probes hold significant promise in various diagnostic applications, including cancer detection, tissue oxygenation monitoring, and inflammation imaging.[78] Their ability to visualize molecular targets non-invasively and in real time provides a powerful tool for assessing disease progression and evaluating therapeutic outcomes. The continued evolution of PA probes, with ongoing improvements in sensitivity, specificity, and versatility, is expected to further solidify their role in advancing personalized medicine and clinical diagnostics.[76]

As mentioned before, different types of PA probes have been introduced. For instance, to detect liver fibrosis a novel fluoro-photoacoustic probe was designed with NIR fluorescence and PAI capabilities. The probe integrated a thioxanthene-hemicyanine dye, which serves as both fluorophore and PA

signal enhancer, and is specifically activated by gamma-glutamyltransferase (GGT), an enzyme known to be involved in liver fibrosis. The probe was functionalized with a cRGD peptide, enabling selective targeting of fibrotic liver tissue *via* integrin binding. Upon enzymatic cleavage by GGT, fluorescence and PA signals of the probe were significantly enhanced, providing sensitive and specific imaging of liver fibrosis. This probe demonstrated a 36-fold increase in fluorescence intensity at 770 nm and a 3.0-fold enhancement in PA intensity at 730 nm, confirming the successful activation by GGT. The high-performance liquid chromatography (HPLC) analysis revealed that GGT cleaved the probe at the glutamic acid site, releasing

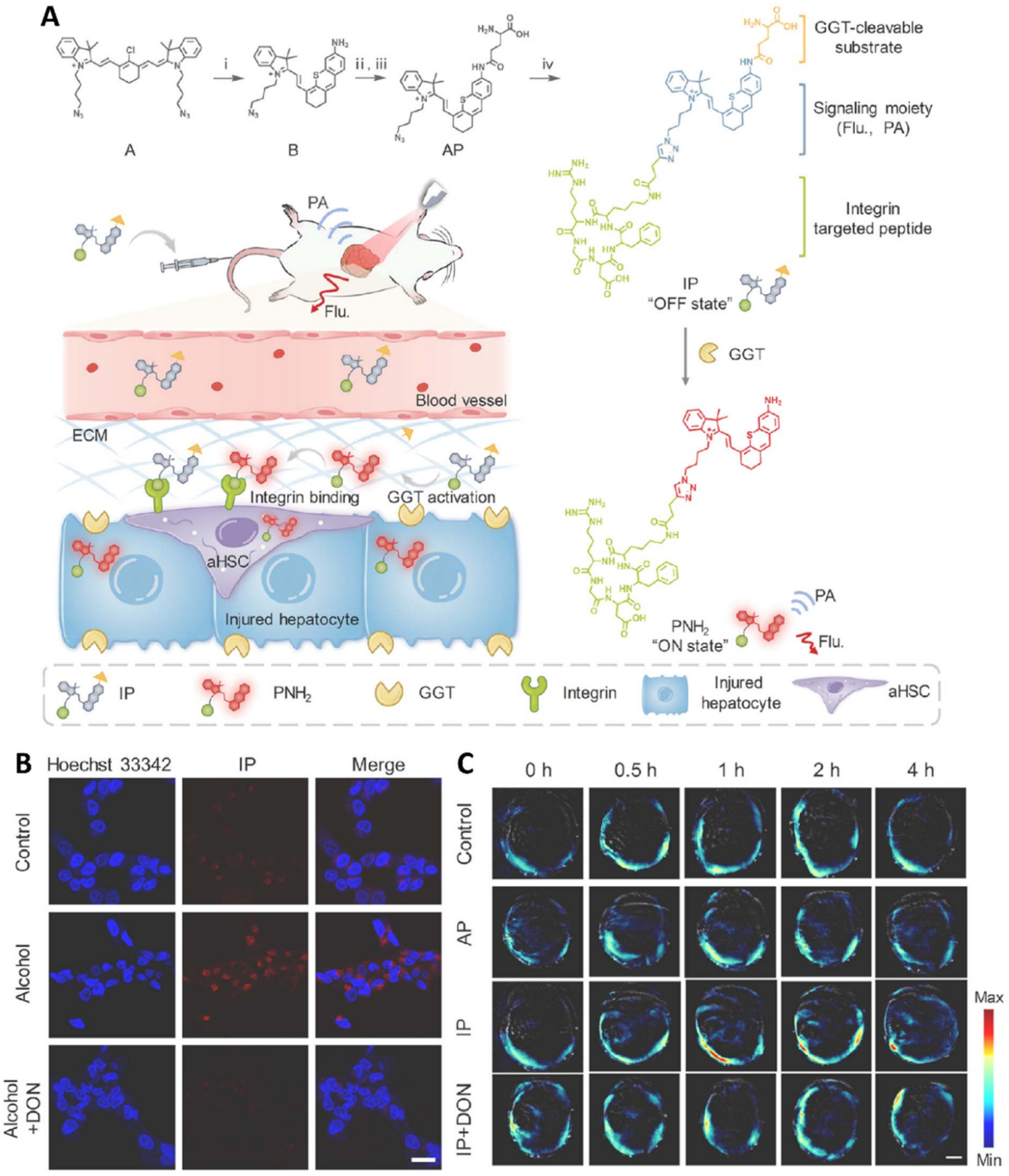

Fig. 7 (A) Schematic diagram showing IP for near-infrared fluoro-photoacoustic imaging of early-stage liver fibrosis. (B) Fluorescence images of LO2 cells treated with IP (15 μM) or pre-treated with GGT inhibitor DON (1 mM) before IP treatment. Scale bar: 20 μm. (C) PA images of mice after intravenous injection of IP or AP, with liver fibrosis mice pre-treated with DON. Scale bar: 5 mm. Reproduced from ref. 79 with permission from Elsevier B.V, copyright 2023.

the active form, which then exhibited the enhanced imaging capabilities. Moreover, no significant signal enhancement was observed when probe was incubated with other proteases, indicating its high selectivity for liver fibrosis. The biocompatibility of probe was assessed using hepatocyte cell lines that showed no significant toxicity, and its long-term photostability under light exposure further validated its potential for prolonged use in imaging applications. In a liver injury model, the probe effectively detected GGT activity in liver cells treated with alcohol, showing its ability to monitor fibrosis at the cellular level. Furthermore, *in vivo* imaging in murine models successfully identified fibrotic regions in the liver, where the cRGD peptide played a crucial role in enhancing tissue-specific targeting (Fig. 7).[79] Therefore, the fabricated probe showed great potential for non-invasive, real-time detection of liver fibrosis. The combination of fluorescence sensitivity with the deeper tissue penetration of PAI enhanced the accuracy of diagnosis and monitoring. This innovative approach could offer improved biocompatibility and accuracy, making it a promising tool for clinical applications in liver fibrosis detection.

A targeted PA probe was fabricated in another research for the detection of inflammation in the prefrontal cortex (PFC) of a lipopolysaccharide (LPS)-induced neuroinflammation mouse model. The probe (MSINPs) was fabricated *via* coating silica NPs (SiNPs) with macrophage cell membranes and doping them with the NIR-II dye IR1061 that demonstrated enhanced inflammation specificity, prolonged blood circulation, and good biocompatibility both *in vitro* and *in vivo*. The targeting ability of MSINPs was evaluated *in vitro* by testing their interaction with LPS-treated human umbilical vein endothelial cells (HUVECs), which were used to simulate inflammation. Results showed that MSINPs were more efficiently internalized by LPS-treated HUVECs than untreated cells, which was attributed to the macrophage membrane proteins, such as Mac-1 and VLA-4, which facilitate targeting of the inflammatory cells. Results of western blot analysis confirmed the presence of integrin β1 and cluster of differentiation 11b (CD11b), indicating that the MSINPs maintained the inflammatory targeting ability of macrophages. The fabricated NPs exhibited excellent biocompatibility, as confirmed by *in vitro* cytotoxicity assays, which showed negligible toxicity to both HUVECs and macrophage-like cells. The MSINPs did not induce significant cell death or morphological changes, indicating their safe use for *in vivo* applications. *In vivo* experiments were conducted using a subcutaneous inflammation model in mice, where LPS was injected into the induce localized inflammation. After intravenous administration of MSINPs, the fluorescence signal in the LPS-injected region was significantly stronger compared to the control PBS-injected region, suggesting that the MSINPs were effectively accumulated in the inflamed areas. Moreover, the fluorescence intensity of MSINPs was higher than that of uncoated SINPs, indicating that coating with macrophage membrane enhanced NP targetability toward the inflammation sites. Furthermore, the NPs maintained their stability and did not cause adverse effects *in vivo*, suggesting they are suitable for long-term circulation and inflammation imaging in animal models (Fig. 8).[80]

A molecular probe, Z-GGRFF-IR775, was developed to detect urokinase plasminogen activator (uPA) activity in breast cancer through fluorescence and photoacoustic imaging (PAI). The probe was designed to become fluorescent upon enzymatic cleavage by uPA, which is typically overexpressed in invasive breast cancers. *In vitro* enzyme assays confirmed the probe's activation mechanism, showing a marked increase in fluorescence following cleavage by uPA, thus validating its specificity and functionality. Researchers further evaluated the performance of prob using breast cancer cell lines. In the presence of uPA, the probe exhibited a substantial fluorescence signal, confirming its ability to respond to the enzymatic activity in a cellular environment. *In vivo* fluorescence imaging showed strong signal enhancement specifically in tumors with high uPA expression, creating a clear and distinguishable contrast between cancerous and non-cancerous tissues. Moreover, PAI revealed robust signals at the tumor site, validating the dual-modality imaging capabilities of probe. By combining fluorescence sensitivity with the deep tissue resolution of PAI, the probe enabled accurate tumor localization and real-time activity monitoring. This dual imaging strategy offered detailed insight into tumor biology and showed significant potential for early cancer detection and evaluation of therapeutic responses. The ability of Z-GGRFF-IR775 to selectively highlight cancerous tissue based on uPA activity underscored its promise for improving diagnostic precision in breast cancer.[81]

The photoacoustic, ultrasound, and angiographic tomography (PAUSAT) platform was developed as a novel tri-modal imaging system integrating PAI, ultrasound (US), and acoustic angiography (AA) to provide non-invasive, high-resolution structural, vascular, and molecular imaging in small animals. Each modality served a distinct role: US captured fine anatomical details, AA provided enhanced vascular contrast, and PAI delivered functional and molecular insights based on optical absorption. Simultaneous acquisition and co-registration of the three modalities enabled more comprehensive visualization. Phantom experiments confirmed the strengths of each technique, US offered sharp tissue outlines, AA delivered high-contrast vascular imaging, and PAI revealed molecular composition. In live animal imaging, PAI demonstrated a superior contrast-to-noise ratio (14.38) compared to US (3.01), clearly highlighting tumor-specific signals. AA contributed detailed vascular mapping, while 3D image reconstruction revealed integrated views of organs, vessels, and tumors. The system also proved useful in monitoring pregnancy, accurately measuring embryonic crown-rump length and placental size in alignment with expected developmental benchmarks. Sensitivity tests using the BIBDAH NIR-II dye showed the platform could detect concentrations as low as 3 $\mu g\ mL^{-1}$. Importantly, PAI was able to suppress hemoglobin interference, isolating signals from BphP1-tagged tumors, which precisely overlapped with locations identified by US, confirming the reliability of PAI in molecular targeting.[82] By combining structural, vascular, and molecular imaging, this approach provides a more comprehensive understanding of biological processes and could prove to be a valuable asset in preclinical research.

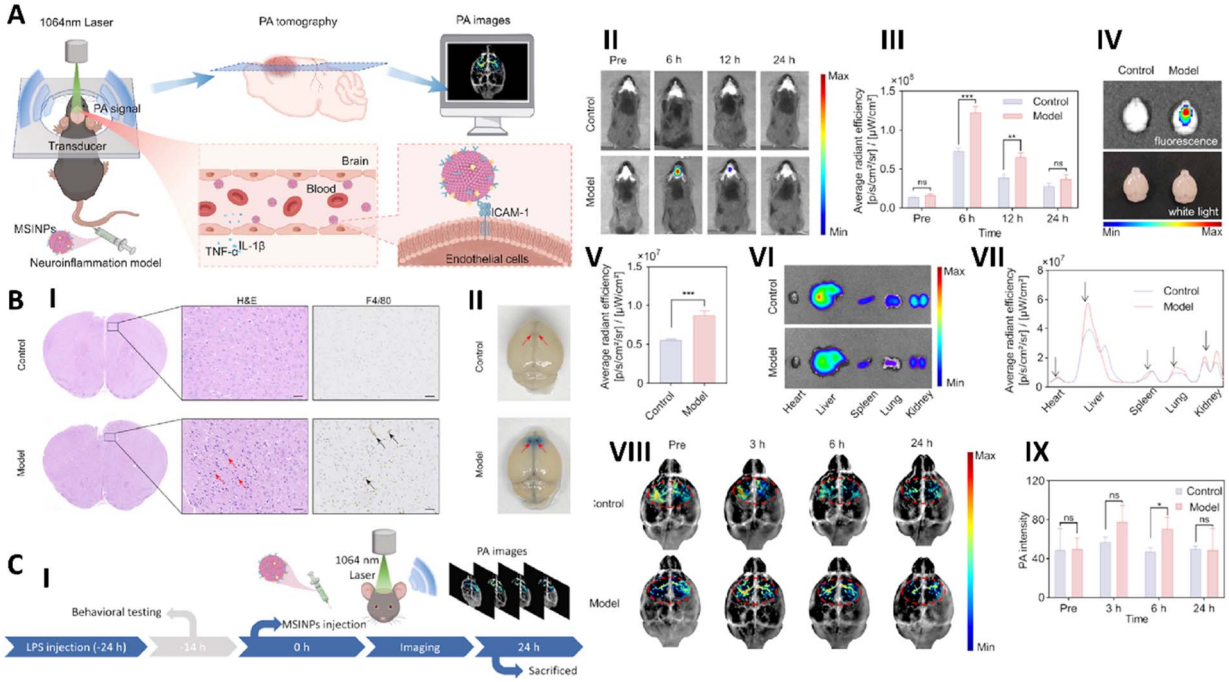

Fig. 8 (A) Schematic image the design of macrophage membrane-coated silica NPs (MSINPs) for photoacoustic imaging of neuroinflammation. (B) Images of (I) H&E and immunofluorescence staining (of the prefrontal cortex (PFC) regions in mouse brains 24 hours after LPS or saline injection) and (II) Evans blue dye staining (of whole brains). (C) Schematic image related to the experimental procedure used for the establishment of LPS-induced neuroinflammation mice model (I). Results of the accumulation of MSINPs in mice (control and neuroinflammation models) during 24 h, fluorescence image (II) and quantitative data (III). Fluorescence image (IV) and quantitative data (V) of brains of control and neuroinflammation mice after 24 h MSINPs injection. Result of accumulation of MSINPs in vital organs after 24 h of injection, (VI) fluorescence image (VII) and quantitative data. Results of PAI (VIII) and quantitative data (IX) of control and neuroinflammation mice injected with MSINPs during 24 h. Reproduced from ref. 80 with permission from American Chemical Society, copyright 2024.

PAI combines optical and ultrasound modalities to provide high-resolution imaging of deep tissues. Molecular probes like macrophage membrane-coated silica NPs (MSINPs) and cRGD-functionalized dyes for liver fibrosis detection demonstrate the precision of PAI in targeting disease-specific biomarkers. For instance, fluoro-photoacoustic probes designed to detect gamma-glutamyltransferase activity in fibrotic livers combine fluorescence and PAI to enhance imaging specificity. These advancements highlight the dual potential of PAI probes for both diagnostics and therapeutic monitoring.

2.5. Fluorescence molecular imaging probes

Fluorescence molecular imaging (FMI) probes are essential for the non-invasive visualization of molecular markers associated with diseases, providing high sensitivity and real-time imaging.[83] These probes typically consist of a fluorescent dye or fluorophore conjugated to targeting moieties, such as antibodies, peptides, or small molecules, enabling them to bind selectively to specific biomarkers.[83,84] In the context of cancer imaging, FMI probes can detect molecular alterations at the cellular and tissue levels, offering the potential for early detection and precise monitoring of disease progression.[85] One of the key advantages of fluorescence imaging is its ability to provide high-resolution images with minimal tissue damage, making it an attractive technique for both diagnostic and therapeutic applications.[84]

Fluorescent probes can be classified into several categories based on their structure and mode of action. Small molecule probes are commonly used to target specific receptors or proteins that are overexpressed in tumors, facilitating the detection of cancerous tissues.[86] These probes are advantageous due to their small size, which allows for efficient tissue penetration. However, challenges remain in distinguishing tumor-specific signals from background fluorescence in surrounding tissues.[87] To address this issue, NP-based probes, such as quantum dots (QDs), graphene quantum dots (GQDs), and Au NPs, have been developed. These NPs offer enhanced fluorescence properties due to their unique size-dependent optical characteristics and can be functionalized with ligands to target specific tumor biomarkers, thereby improving imaging sensitivity and reducing background noise.[88–90] Additionally, activatable probes have gained attention for their ability to remain non-fluorescent until they encounter their target.[91] This feature significantly reduces background interference, improving imaging contrast and specificity. For example, OTL-38, a folate receptor-targeted activatable probe, remains non-fluorescent until it interacts with folate receptors, making it particularly useful for tumor imaging with minimal background signal.[91] These probes are particularly valuable in clinical applications, such as fluorescence-guided surgery (FGS), where real-time imaging is crucial for accurate tumor delineation.[92] Probes like BLZ100, which targets matrix metalloproteinase-2 (MMP2)

in tumors, can assist surgeons in distinguishing tumor tissue from healthy tissue, thus enhancing surgical precision and reducing the risk of recurrence.[86,93]

Overall, fluorescence molecular imaging probes are crucial in advancing non-invasive diagnostic and treatment methods. Researchers are focusing on creating probes that are more specific, sensitive, and versatile, aiming to improve their use in cancer detection, guiding surgery, and personalized treatment. As research continues, FMI probes are expected to enhance diagnostic accuracy, minimize side effects of treatment, and ultimately lead to better outcomes for cancer patients.

A novel organic molecular probe, Lipi-QA, was produced in a study, for high-resolution imaging of lipid droplets (LDs) in living cells using stimulated emission depletion (STED) microscopy. The probe was specifically designed to address key limitations of conventional LD imaging probes, such as photostability, LD specificity, and fluorescence lifetime. It was observed that increasing the laser intensity progressively sharpened the LD images, with the highest resolution achieved at a laser intensity of 5 MW cm^{-2}, reaching a resolution of approximately 37 nm, far surpassing the diffraction limit of light (~250 nm). This exceptional resolution led to visualizing the fission process of LDs, for the first time, where a spherical droplet elongated and split into two smaller droplets. Additionally, time-lapse STED imaging was employed to study the dynamics of LDs under starvation conditions that led to changes in the size and movement of LDs over time. Specifically, it was found that the size of LDs increased after prolonged starvation, suggesting that autophagy of other cellular organelles contributed fatty acids to enlarge the residual LDs. The

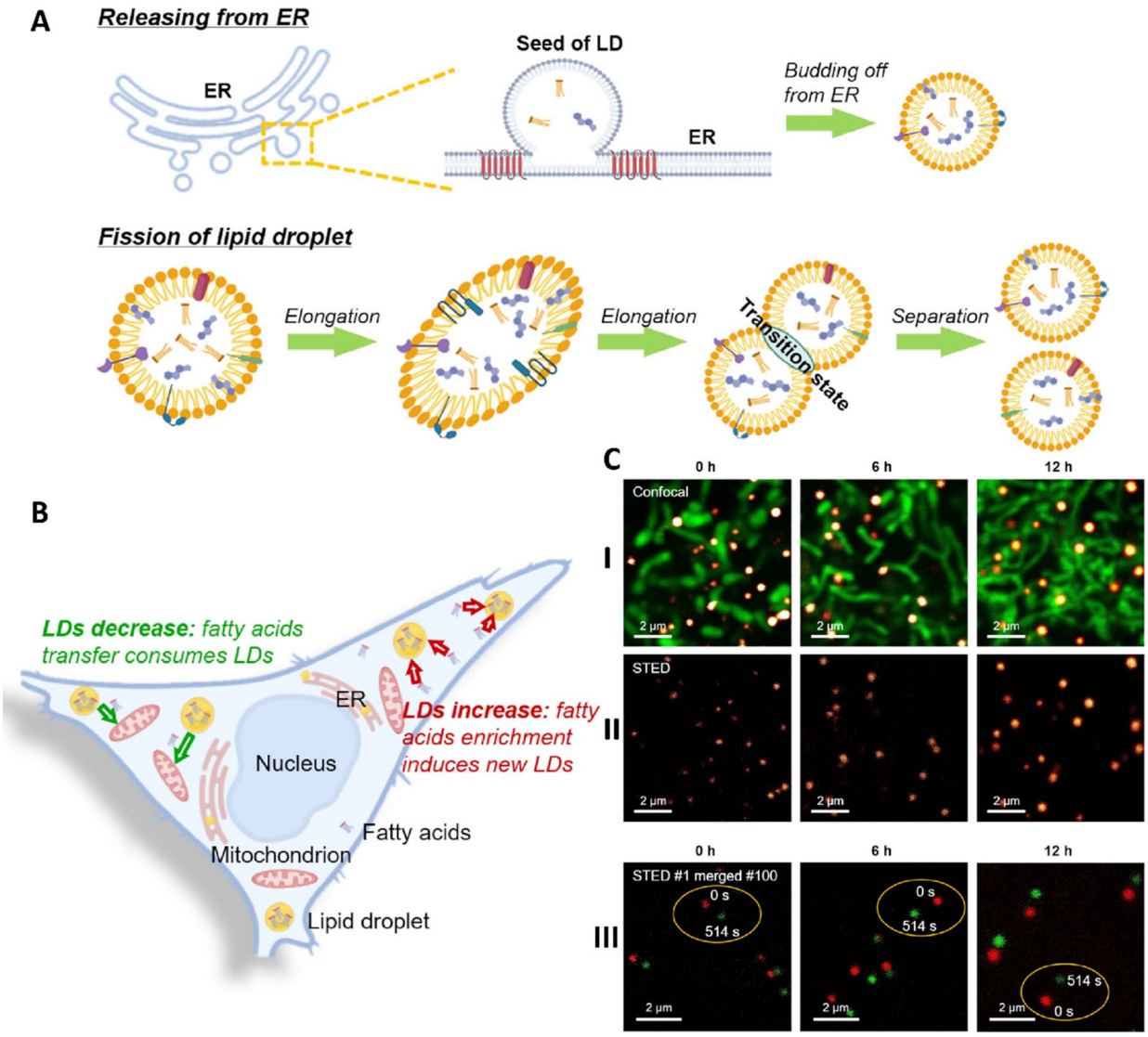

Fig. 9 (A) Schematic representation of the two proposed mechanisms for lipid droplet (LD) formation. (B) Controversial question regarding whether the number of LDs increases or decreases during starvation (C) (I & II) Confocal and STED super-resolution images of living HeLa cells under starvation at different time points. (III) Merged images showing the first (0 s) and last (514 s) frames from time-lapse STED super-resolution imaging of living HeLa cells under starvation. Scale bar: 2 μm. Reproduced from ref. 94 under the Creative Commons Attribution License. Ivyspring International Publisher, copyright 2023.

movement speed of the droplets also increased after 6 h of starvation, likely reflecting enhanced lipid metabolism under nutrient deprivation. This study demonstrated the ability of Lipi-QA to provide unprecedented insight into LD behavior at the nanoscale, including the visualization of dynamic processes such as LD fission and changes in size and movement under stress conditions (Fig. 9).[94] By incorporating high photostability, LD specificity, and a long fluorescence lifetime, this probe can enable precise, nanoscale imaging using STED microscopy. Such an approach has the potential to provide novel insights into cellular lipid metabolism and organelle dynamics, opening the way for advancements in understanding disease mechanisms and facilitating drug discovery efforts.

A simple and highly sensitive method was developed in a study for detecting PD-L1-positive exosomes with high specificity. Au nanospheres (GNSs) were electrostatically adsorbed onto the bottom of an eight-well chambered slide to create a detection substrate. Cy5-labeled CD63 aptamers were then anchored to the GNSs *via* Au–S bonds to act as capture probes. After introducing DiI-stained exosome samples, FAM-labeled PD-L1 aptamers (immunoprobes) were added to specifically bind PD-L1 on the exosome surface. Detection was achieved through triple-color fluorescence co-localization (TFC) using Cy5, DiI, and FAM channels, enabling highly specific and sensitive identification of PD-L1-expressing exosomes across concentrations from 7.78×10^1 to 7.78×10^4 particles per mL, with a detection limit as low as 6 particles per mL. Based on a series of experimental results, the optimal detection conditions were established, and the biosensor was found to be stable, reproducible, and capable of detecting exosomes in complex biological samples. This highly sensitive and specific immunoassay provided a simple and cost-effective approach for identifying tumor-derived exosomes, showing strong potential for applications in biomedical research and diagnostics. It was a simple to fabricate and clean detection substrate, and the TFC strategy effectively eliminated nonspecific signals, significantly improving accuracy.[95]

The PD-1/PD-L1 pathway has emerged as a promising strategy in cancer immunotherapy, yet variable response rates and the risk of hyperprogression following treatment highlighted the need for better patient selection. To address this, molecular imaging, particularly NIR fluorescence imaging, was explored as a noninvasive method to dynamically monitor PD-L1 expression *in vivo*. In this context, a novel PD-L1-targeting peptide antagonist, AUNP-12, was developed and conjugated with Cy5.5 and CH1055 for NIR-I and NIR-II imaging, respectively. These probes successfully visualized PD-L1 expression across different mouse tumor models, offering insights into tumor-immune dynamics. In 4T1 tumor models characterized by low PD-L1 expression, AUNP-12-CH1055 achieved superior tumor visualization compared to the NIR-I probe, due to reduced background fluorescence and deeper imaging capability. To further assess the probe's ability to detect PD-L1 heterogeneity, mice were implanted with both MCF-7 and MDA-MB-231 cells in opposite mammary glands. The probe preferentially accumulated in MDA-MB-231 tumors, reflecting its specificity for PD-L1 and confirming its potential to distinguish tumors based on expression levels. AUNP-12-Cy5.5 demonstrated enhanced targeting of MDA-MB-231 tumors with high PD-L1 expression, while showing lower uptake in MCF-7 tumors, which express PD-L1 at lower levels. These results support the utility of AUNP-12-based probes for guiding immunotherapy through real-time imaging, patient stratification, and noninvasive assessment of tumor heterogeneity.[96]

In a research, a series of curcumin-derived fluorescent dyes was developed for live-cell imaging, with a focus on their application in fungal systems. Structural modifications involved adding electron-donating groups to the curcumin backbone, enabling tunable fluorescence emissions across a broad spectral range (470–690 nm). These substitutions induced red shifts in both absorption and emission spectra, enhancing brightness and quantum yields (6–98%), especially for derivatives with stronger donor groups. The improved photophysical performance was attributed to the increased push–pull electronic effect. Since the dyes were water-insoluble, photophysical properties were evaluated in organic solvents such as THF. Cytotoxicity tests conducted on *Fusarium oxysporum* showed no toxic effects at concentrations up to 100 μM over a 7-day period, indicating good biocompatibility. Confocal microscopy confirmed successful internalization of the dyes into fungal cells, where they selectively accumulated in specific subcellular compartments. The dyes exhibited distinct emission colors, blue, green, and red, depending on their structure, enabling multicolor imaging and co-staining capabilities. Clear, low-background fluorescence signals further supported their suitability for high-resolution imaging. Notably, different dyes showed similar organelle-targeting behavior, a valuable trait for multiplexed visualization. Unlike traditional fungal stains that are limited to single-color emission, these curcumin-based dyes offer a versatile platform for detailed and dynamic studies of fungal cell architecture.[97] Therefore, utilizing curcumin-based fluorescent dyes for live-cell imaging leveraging their excellent photophysical properties such as broad emission spectra and high fluorescence efficiency. These dyes could selectively target sub-cellular compartments and support multi-color co-staining, making them versatile for biological imaging and so this approach holds promise for advancing research in fungal cell biology, organelle function, and cellular dynamics.

$SeCF_3$-IRD800, a NIR-II fluorescence imaging probe, was developed to target HDAC6, a histone deacetylase subtype overexpressed in liver cancer. The probe was synthesized by linking a selective HDAC6 inhibitor ($SeCF_3$) to the fluorescent dye IRDye800cw. Designed for liver cancer imaging and fluorescence-guided surgery (FGS), $SeCF_3$-IRD800 was evaluated in mouse models with liver fibrosis and orthotopic liver tumors to assess its tumor-targeting specificity. Following intravenous injection, the probe selectively accumulated in tumor tissue, with minimal uptake in normal liver, enabling clear tumor visualization. The fluorescence signal peaked at 8 hours post-injection, achieving a high tumor-to-background ratio (TBR), even in fibrotic liver environments. Importantly, the probe's fluorescence intensity strongly correlated with HDAC6 expression levels ($R^2 = 0.8124$), confirming its targeting specificity. $SeCF_3$-IRD800 also demonstrated the ability to detect sub-2 mm

tumors not visible under white light, enhancing intraoperative precision. In human liver cancer tissue samples, the probe showed significantly higher fluorescence in tumors than in adjacent normal tissue. HDAC6 inhibition with SAHA reduced fluorescence intensity, supporting the probe's dependence on HDAC6 activity. Additionally, the probe exhibited low cytotoxicity and minimal background fluorescence in healthy liver tissue, highlighting its safety and suitability for *in vivo* use and potential clinical application in FGS for liver cancer (Fig. 10).[98] Therefore, $SeCF_3$-IRD800 represented a promising tool for liver cancer imaging and fluorescence-guided surgery. Its ability to specifically target HDAC6, a marker of liver cancer, and provide clear visualization of tumor margins even in the presence of liver fibrosis or cirrhosis makes it highly suitable for clinical applications. Based on these results, the probe could address key limitations of existing imaging agents, such as high liver background signals, offering better accuracy and efficiency in liver cancer surgery. However, further studies are needed to explore its sensitivity, long-term safety, and broader clinical applicability.

To overcome challenges such as cytotoxicity, structural complexity, and limited specificity in intracellular RNA imaging, researchers developed three cationic molecular rotors, OX-JLD (oxygen-based julolidine–azolium conjugate), BTZ-JLD (sulfur-based julolidine–azolium conjugate), and SEZ-JLD (selenium-based julolidine–azolium conjugate), based on a julolidine–azolium framework. Each rotor featured a "push–pull" architecture, combining an electron-donating julolidine group with an electron-withdrawing benzo-azole cationic moiety, linked by a π-conjugated spacer. Oxygen, sulfur, or selenium atoms were incorporated to tune the optical performance of dyes, aiming to improve water solubility, nucleolar targeting, and red-region emission. Among the probes, SEZ-JLD (the selenium variant) showed the most promising results. Selenium incorporation enhanced electron transfer and charge stabilization, leading to superior optical features. SEZ-JLD exhibited deep-red fluorescence, advantageous for biological imaging due to reduced autofluorescence and improved tissue penetration. Spectral analysis confirmed red-shifted absorption and emission compared to its oxygen- and sulfur-based counterparts, making it better suited for red/NIR imaging. The fluorescence property of probe was strongly increased upon RNA binding, with minimal sensitivity to viscosity, ensuring RNA-specific detection. SEZ-JLD also demonstrated excellent biocompatibility, maintaining over 85% cell viability at higher concentrations, confirming its suitability for live-cell imaging. Live-cell experiments revealed strong, nucleolus-specific fluorescence, confirming selective RNA binding without background interference. SEZ-JLD readily penetrated cell membranes without auxiliary agents, streamlining its use. While OX-JLD and BTZ-JLD also targeted RNA, they showed lower emission intensity and shorter wavelengths, making SEZ-JLD the most effective option for deep-tissue and high-contrast RNA imaging.[99]

A near-infrared fluorescence (NIRF) molecular probe was developed by conjugating the EGFR-targeting monoclonal antibody cetuximab with the Cy7 dye, aiming to enhance visualization of epithelial ovarian cancer (EOC) during fluorescence-guided surgery (FGS). The dye was attached to lysine residues on cetuximab, and an isotype IgG was used as a control to assess nonspecific binding. The successful conjugation preserved the fluorescence properties of Cy7 for real-time imaging. Immunohistochemical analysis of patient tissue microarrays revealed significantly higher EGFR expression in EOC tissues compared to normal fallopian tube samples, supporting EGFR as a suitable imaging target. Further examination of various ovarian cancer cell lines revealed that SKOV3 cells had the highest expression of EGFR, confirming them as an ideal candidate for further *in vivo* studies. *In vivo* imaging demonstrated that the probe successfully targeted the tumors and produced clear fluorescence signals, with excellent tumor-to-background (T/B) ratios, particularly when administered at higher doses of 10 μg and 30 μg. The results indicated that the cetuximab-Cy7 probe had no significant cytotoxic effects at the concentrations used for imaging, demonstrating that the conjugate did not adversely affect cell viability. This finding was crucial, as it suggested that the probe could be safely used for imaging without inducing any side effects to the tumor cells, which is a key consideration when developing molecular probes for clinical use. Overall, the cetuximab-Cy7 conjugate showed promise as a safe and effective tool for EGFR-targeted imaging in EOC, potentially improving tumor margin detection and surgical outcomes.[100]

A novel covalent organic nanosheet (CON) system, TpPy CONs, was developed for bioimaging applications *via* synthesizing TpPy covalent organic frameworks (COFs) through Schiff base condensation of 1,3,5-triformylphloroglucinol and 2,7-diaminopyrene, followed by exfoliation in water *via* ultrasonication. The resulting CONs exhibited strong fluorescence at 781 nm upon 633 nm excitation, attributed to the reduced π–π stacking after exfoliation. With particle sizes below 200 nm and thickness under 1.7 nm, the nanosheets demonstrated excellent suitability for cellular uptake. Biocompatibility assessments revealed low cytotoxicity, maintaining over 90% cell viability at concentrations up to 50 μg mL^{-1} in MDA-MB-231 and RAW 264.7 cells. *In vitro* imaging confirmed successful internalization and intense intracellular red fluorescence. *In vivo* studies using tumor-bearing mice showed substantial tumor accumulation driven by the enhanced permeability and retention (EPR) effect, with fluorescence signals significantly stronger than both TpTTA CONs and other NP formulations. These findings indicated the strong potential of TpPy CONs for high-performance bioimaging in both cellular and whole-body contexts.[101]

Eco-friendly carbon quantum dots (CQDs) were synthesized from biomass waste using a one-pot hydrothermal method. The resulting CQDs, derived from citric acid, palm kernel shell, and oyster shell, had small sizes (<10 nm), strong biocompatibility, and tunable, excitation-dependent fluorescence emission. These CQDs exhibited bright, stable fluorescence, making them suitable for bioimaging applications. Notably, fluorescence imaging using confocal microscopy confirmed efficient cellular uptake of CQDs across multiple cell lines, including human dermal fibroblasts, HeLa, cardiomyocytes, and iPSCs. *In vivo* fluorescence imaging in medaka fish embryos and larvae

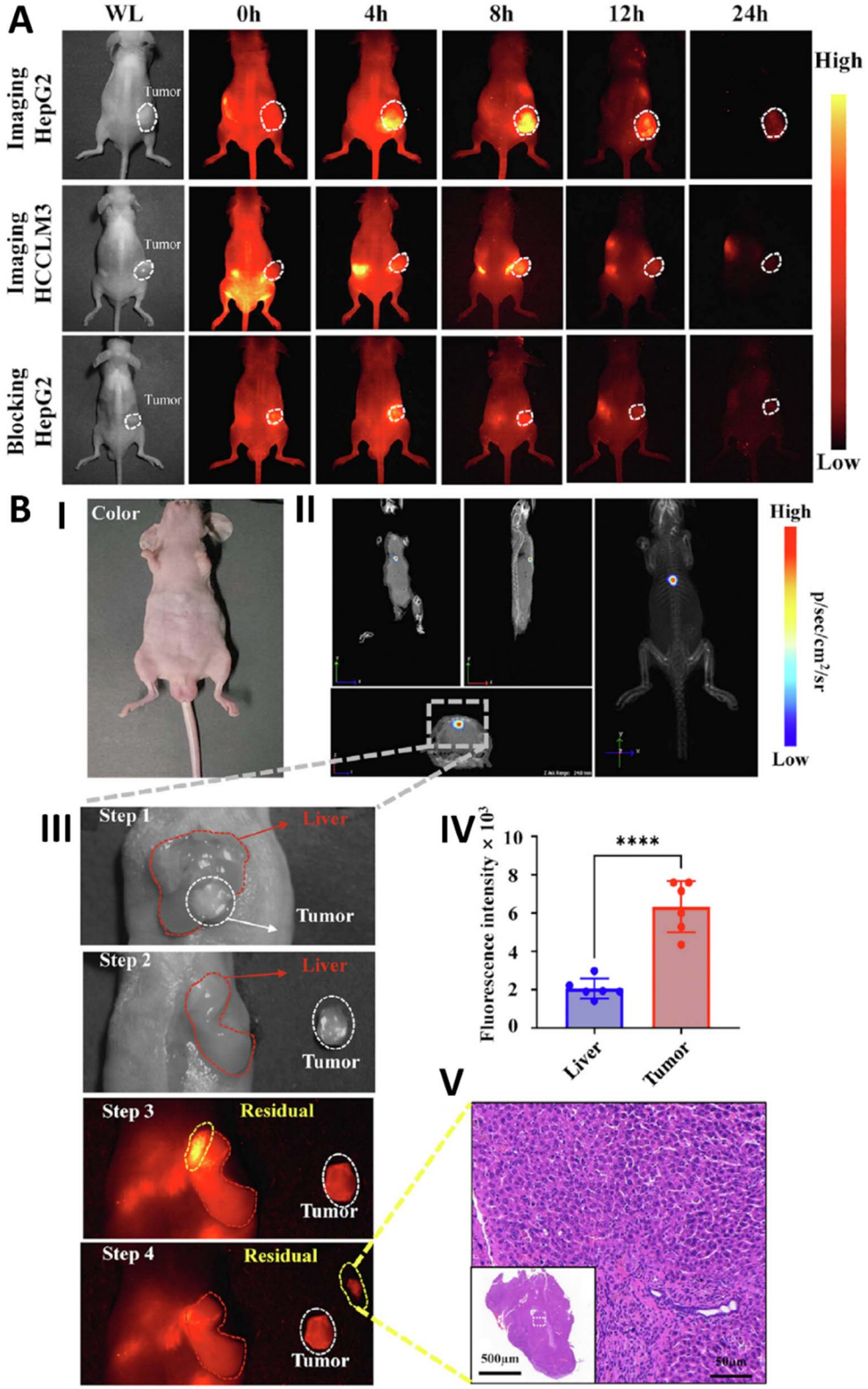

Fig. 10 (A) NIR-II imaging at various time points following intravenous injection of $SeCF_3$-IRD800 in HepG2-Luc and HCCLM3 subcutaneous xenograft tumor models ($n = 12$), as well as in HepG2-Luc subcutaneous tumor blocking experiments ($n = 6$). (B) (I) 3D reconstruction of the tumor using LI-CT (tumor area indicated by the gray dashed wireframe). (II) Fluorescence-guided surgery process: Step 1: white light examination for HCC lesions; Step 2: first resection under white light; Step 3: NIR-II fluorescence-guided examination for residual lesions; Step 4: removal of residual lesions. (III) Pathological evaluation of all residual lesions. Reproduced from ref. 98 with permission from Elsevier B.V, copyright 2023.

further demonstrated the biodistribution and non-toxicity of the probes. Functionally, these CQDs were stimuli-responsive, showing significantly increased uptake in cells pre-treated with tumor necrosis factor-α (TNF-α), a hallmark of inflammation. This feature allowed clear fluorescent visualization of inflamed cells. Moreover, gene expression analysis revealed that citric acid-derived CQDs could reduce levels of the pro-inflammatory cytokine IL-6, suggesting potential anti-inflammatory effects beyond imaging.[102] These findings demonstrate that biomass-derived CQDs serve as theranostic nanoprobes, capable of both high-resolution fluorescence imaging and potential immunomodulatory therapy. Compared to conventional semiconductor quantum dots, carbon-based CQDs offer advantages such as lower toxicity, sustainable synthesis, photostability, tunable emission, and cost-effectiveness, making them promising candidates for future clinical translation in inflammation-related diseases.

A multicolor CQD-based fluorescent probe was produced for targeted imaging of hepatic stellate cells on liver frozen sections at sub-zero temperatures. Three types of water-soluble CQDs (emitting blue, green, and yellow fluorescence) were produced using a green hydrothermal synthesis approach with size between 3.2–4.3 nm and quantum yields of 36.1%, 26.3%, and 21%, respectively. These CQDs exhibited high fluorescence stability, strong photobleaching resistance, and excitation-wavelength independence, key advantages over traditional organic dyes and heavy-metal QDs. Notably, fluorescence intensity was enhanced at low temperatures (−20 to −30 °C), and the probes maintained their optical performance after repeated freeze–thaw cycles, indicating excellent thermal stability and reversibility. The CQDs were conjugated with antibodies (CDs-Ab) targeting the desmin protein, enabling specific immunofluorescent labeling of hepatic stellate cells. Imaging at −20 °C revealed strong blue fluorescence in labeled cells, while control groups without primary antibody showed no significant signal, confirming high specificity. Flow cytometry further validated labeling efficiency (∼89.2%), comparable to commercial FITC-conjugated antibodies. Importantly, even at high concentrations (up to 200 μg mL^{-1}), the probes displayed low cytotoxicity (>80% viability), and high selectivity was demonstrated in frozen liver sections. The results highlight these CQDs as promising fluorescent nanoprobes for stable, low-temperature, cell-specific imaging, particularly useful in studying liver disease pathology at the cellular level.[103]

Fluorescence molecular imaging probes offer real-time, non-invasive visualization of disease-specific biomarkers. Probes functionalized with targeting peptides or antibodies, like hCAIX-targeting liposomes, improve specificity for tumor imaging while enabling targeted drug delivery. *In vivo* fluorescence imaging studies demonstrate the efficacy of these probes in enhancing contrast and reducing off-target effects. By integrating novel fluorophores and responsive designs, fluorescence probes are becoming essential tools for monitoring therapeutic outcomes and advancing personalized medicine.

3 Challenges

The field of molecular imaging (nano)probes is rapidly advancing, yet it faces a myriad of challenges that must be addressed to facilitate successful implementation in clinical diagnostics. An in-depth exploration of these challenges reveals the complexities involved in developing and deploying these innovative tools. Despite the promising developments in MRI molecular probes, several challenges remain. The synthesis of highly specific and biocompatible probes is essential to minimize off-target effects and ensure safety in clinical applications. Additionally, the regulatory pathway for novel contrast agents can be complex, requiring extensive safety and efficacy data before approval.[5,104] For PET, several challenges persist in the use of PET molecular probes. The production of radiolabeled compounds often requires specialized facilities and equipment, which can limit accessibility. Notably, the short half-life of many radionuclides poses logistical challenges for their use in clinical settings, necessitating efficient synthesis and distribution processes. Furthermore, the high cost associated with PET imaging and the need for trained professionals to interpret the results can restrict its widespread implementation.[105] On the other hand, several challenges remain in the use of CT molecular probes. The potential for adverse reactions to contrast agents, particularly in patients with compromised renal function, is a concern that necessitates careful patient selection and monitoring. Moreover, the radiation exposure associated with CT imaging raises safety concerns, particularly with repeated imaging sessions. Efforts to develop safer, lower-dose imaging protocols and alternative contrast agents are ongoing but require further research.[106] Despite the significant advancements, some important challenges remain in the clinical translation of photoacoustic molecular imaging probes. One major hurdle is the need for standardized protocols for probe synthesis, imaging procedures, and data analysis. Notably, while photoacoustic imaging offers high resolution, its penetration depth is still limited compared to traditional imaging modalities such as MRI or CT, which can restrict its applicability in certain clinical scenarios. Furthermore, the reproducibility of results and the long-term stability of probes in biological systems require careful evaluation.[107,108] Despite its advantages, several challenges exist in the implementation of fluorescence molecular imaging. One primary concern is the issue of tissue autofluorescence, which can obscure the signal from fluorescent probes and complicate image interpretation. Additionally, the limited tissue penetration of visible light can restrict the use of fluorescence imaging in deep tissues, necessitating the development of near-infrared probes that can penetrate tissues more effectively. Moreover, regulatory hurdles and the need for standardization in probe design and imaging protocols can slow the adoption of fluorescence imaging in clinical practice.[109,110]

Overall, some of the important challenges in molecular imaging (nano)probes are summarized below:

3.1. Biocompatibility and toxicity

The safety of molecular imaging (nano)probes is paramount. Biocompatibility concerns arise from the potential toxicity of

NPs, which can provoke inflammatory responses or cytotoxicity.[111] Different cell types may react differently to the same probe, making it difficult to predict how they will behave *in vivo*. Moreover, the surface properties of NPs can significantly influence their interactions with biological systems. For instance, surface modifications intended to enhance targeting can inadvertently affect biocompatibility. Researchers must therefore conduct thorough toxicity assessments, including long-term studies to evaluate chronic exposure effects.[112,113]

3.2. Targeting efficiency

Achieving optimal targeting efficiency is complex and involves several factors. The biological environment is dynamic, and the expression levels of biomarkers can vary not only among different patients but also within the same tumor. This heterogeneity complicates the design of probes that can consistently bind to their targets. Moreover, biological barriers such as the extracellular matrix, cellular membranes, and biological fluids can impede the delivery and efficacy of these probes. Advances in nanotechnology, such as the development of smart probes that can respond to specific stimuli, may help improve targeting precision.[114]

3.3. Stability and shelf life

The stability of molecular imaging probes is a critical concern, as their performance can degrade over time or under specific conditions. Environmental factors such as temperature, pH, and ionic strength can affect the stability of NPs. For instance, many NPs may aggregate in physiological conditions, which can diminish their imaging capabilities and alter their pharmacokinetics. Addressing these stability issues requires innovative engineering approaches, such as the use of stabilizing agents or protective coatings that can enhance the resilience of the probes during storage and application.[5,114]

3.4. Regulatory hurdles

The regulatory pathways for nanotechnology-based products can be complex and opaque.[115] Regulatory agencies often require substantial evidence of safety, efficacy, and quality control before approving new imaging agents. This process can be particularly challenging for novel materials, where existing frameworks may not adequately address the unique characteristics and behaviors of nanomaterials. Researchers and developers must engage with regulatory bodies early in the development process to understand requirements and streamline approvals, ensuring that they meet safety standards while encouraging innovation.

3.5. Imaging techniques and integration

The integration of molecular imaging (nano)probes with existing imaging technologies presents additional challenges.[5,113,114,116] Each imaging modality has its own set of requirements and limitations. For instance, while some probes are designed for high sensitivity, they may lack the spatial resolution needed for precise anatomical localization in MRI. Additionally, the need for specialized imaging equipment and trained personnel to operate these systems can create barriers to widespread adoption. Developing hybrid imaging systems that can leverage the strengths of multiple modalities may provide solutions but also adds complexity to probe design.

3.6. Cost and accessibility

The financial implications of developing and deploying molecular imaging (nano)probes are significant.[113,114] High-quality NPs often require costly materials and sophisticated fabrication techniques, which can drive up the price of diagnostic procedures. This is particularly concerning in healthcare systems where budget constraints limit access to advanced technologies. Efforts to scale up production methods, improve manufacturing efficiency, and explore cost-effective materials are essential to enhance accessibility and make these technologies available to a wider patient population.

3.7. Clinical translation

The clinical translation of molecular imaging nanoprobes faces multiple significant challenges that hinder their widespread adoption despite promising preclinical results.[117,118] One major hurdle is the complexity of nanoprobe design, which often involves multifunctional components that can raise safety and toxicity concerns, complicating regulatory approval processes. Achieving consistent large-scale manufacturing with minimal batch-to-batch variability remains difficult, limiting reproducibility and scalability required for clinical use. Additionally, biocompatibility and safety issues are critical, as many nanoprobes accumulate nonspecifically in organs such as the liver and spleen, potentially causing long-term toxicity.[111] The pharmacokinetics and biodistribution of nanoprobes often differ between animal models and humans, complicating the prediction of clinical performance. Furthermore, the cost-effectiveness of nanoprobe-based imaging compared to existing diagnostic methods is a concern, as the development and production expenses are high, while commercial incentives for imaging agents are generally lower than for therapeutics. Regulatory frameworks also pose challenges, as imaging agents require rigorous validation of safety and efficacy, often without expedited pathways available to therapeutics. Notably, the integration of nanoprobes into multimodal imaging platforms demands complex optimization to balance imaging sensitivity with safety and clinical practicality. Addressing these challenges through improved nanoprobe design—such as using biologically inert materials, enhancing targeting specificity, and developing activatable probes—alongside advances in scalable manufacturing and regulatory strategies, is essential to facilitate the successful clinical translation of molecular imaging nanoprobes and realize their full potential in personalized medicine.[117–119] Additionally, robust clinical validation is essential for establishing the utility of molecular imaging (nano)probes in medical diagnostics.[113,114] Clinical trials must demonstrate not only the safety and efficacy of the probes but also their ability to improve patient outcomes compared to existing diagnostic methods. This often requires large-scale

studies across diverse patient populations, which can be resource-intensive and time-consuming. Furthermore, standardizing protocols for probe administration, imaging procedures, and data analysis is crucial to ensure that results are reproducible and comparable across different studies.

4 Future perspectives

The future of molecular imaging (nano)probes in medical diagnostics is bright and filled with potential. Future research directions may focus on the development of more sophisticated probes that incorporate advanced targeting strategies, such as the use of aptamers or nanobodies that exhibit high affinity and specificity for their targets. Moreover, the application of machine learning and AI in analyzing MRI data could enhance the interpretation of images obtained with molecular probes, leading to more accurate diagnoses. For PET, innovations in radiochemistry and the development of new radionuclides may lead to the creation of more sensitive and specific probes that can target a wider range of diseases. Advances in AI and machine learning are expected to enhance image analysis, allowing for improved detection of subtle changes in metabolic activity. Additionally, the continued exploration of PET imaging in combination with emerging therapeutic strategies, such as targeted therapies and immunotherapies, will likely play a pivotal role in personalized medicine, ultimately improving patient management and outcomes. Notably, additionally explorations on CT molecular probes ought to be focused on the development of next-generation contrast agents that offer improved safety profiles and targeting capabilities. Innovations such as multifunctional NPs and the use of biomimetic materials could enhance the efficacy of CT imaging while minimizing risks. Advancements in AI and machine learning are expected to improve image processing and analysis, enabling more accurate interpretations of CT scans. As these technologies evolve, the role of CT molecular probes in personalized medicine is likely to expand, leading to better diagnostic outcomes and more effective treatment strategies. Furthermore, future research ought to be focused on photoacoustic molecular imaging with the purpose of developing more sophisticated probes with enhanced targeting capacity and signal strength. Innovations in bio- and nanomedicine may lead to the emergence of multifunctional probes that combine imaging with therapeutic applications, such as photothermal therapy. Current developments on imaging systems and data processing techniques, including the integration of AI, are expected to improve image reconstruction and analysis, further enhancing the utility of PAI in clinical settings. Furthermore, additional explorations on fluorescence molecular imaging ought to be conducted on development of next-generation probes that offer improved targeting and signal characteristics. Innovations in nanotechnology and bioconjugation techniques may lead to the creation of multifunctional probes capable of simultaneous imaging and therapeutic applications. In this context, advancements in imaging technologies, including the integration of AI for enhanced image analysis, are expected to improve the accuracy and efficiency of fluorescence imaging.

Overall, we can anticipate significant developments that will enhance the effectiveness, accessibility, and application of these probes in clinical settings. Here are several key perspectives on the future of molecular imaging (nano)probes:

4.1. Enhanced targeting and specificity

Future innovations in molecular imaging (nano)probes will likely focus on improving targeting capabilities. Researchers are exploring the use of sophisticated ligands and targeting moieties, such as antibodies, peptides, and aptamers, that can selectively bind to specific biomarkers associated with diseases. The development of "smart" probes that can respond to specific physiological conditions or stimuli (*e.g.*, pH, enzymes, or temperature) will enhance their specificity and reduce off-target effects. This could lead to more accurate imaging and improved diagnostic outcomes.

4.2. Integration of multi-modal imaging

The integration of molecular imaging (nano)probes with multimodal imaging techniques will be a significant trend. By combining different imaging modalities, such as PET, MRI, and fluorescence, researchers can obtain complementary information about biological processes. This hybrid approach will allow for more comprehensive disease assessment, enabling clinicians to visualize and understand complex biological interactions in real-time. As imaging technologies converge, the ability to gather detailed anatomical and functional data simultaneously will significantly enhance diagnostic capabilities.

4.3. Advancements in theranostics

The concept of theranostics, which combines therapeutic and diagnostic functions, will continue to gain traction in the field of molecular imaging. Future nano-probes will be developed to not only visualize disease processes but also deliver targeted therapies. This dual functionality can enhance treatment efficacy while minimizing side effects, as clinicians can monitor therapeutic responses in real-time. As personalized medicine becomes increasingly important, theranostic agents will play a pivotal role in tailoring treatment strategies to individual patients.

4.4. Personalized medicine and biomarker discovery

As our understanding of the molecular basis of diseases improves, molecular imaging (nano)probes will contribute to the identification and validation of novel biomarkers. This will facilitate the development of personalized diagnostic approaches that consider individual patient characteristics, such as genetic profiles and disease stage. By providing precise information about disease states, these probes can guide treatment decisions and improve patient outcomes, making personalized medicine a standard practice in healthcare.

4.5. AI and data analysis

The integration of AI and data analytics into molecular imaging will advance the interpretation of imaging data. Machine

learning algorithms can analyze large datasets generated by imaging studies, identifying patterns and correlations that may go unnoticed by human observers. This can lead to improved diagnostic accuracy, prognostic assessments, and treatment planning. Furthermore, AI can assist in optimizing probe design and imaging protocols, streamlining workflows in clinical settings. Rather than solely focusing on black-box machine learning algorithms, future efforts should prioritize explainable AI approaches that provide transparent decision-making processes. This can enhance clinician trust and facilitate regulatory approval. AI frameworks should be designed to integrate heterogeneous data types—molecular imaging outputs, genomic profiles, clinical records—enabling comprehensive patient stratification and personalized diagnostics. Implementing AI algorithms for real-time noise reduction, artifact correction, and standardization of imaging data will improve reproducibility and diagnostic reliability. Additionally, machine learning models can be trained on large datasets of nanoprobe physicochemical properties and biological outcomes to predict optimal probe configurations, accelerating the design cycle. Developing standardized algorithms and software platforms for seamless fusion of data from PET, MRI, CT, and optical imaging modalities will enhance spatial and functional resolution. Notably, engineering integrated hardware capable of simultaneous acquisition and synchronized data processing will reduce patient burden and improve diagnostic throughput. Furthermore, designing multifunctional nanoprobes that are inherently compatible with multiple imaging modalities will simplify probe administration and improve diagnostic accuracy. Thus, the specific technical pathways for advancing molecular imaging through AI and multimodal integration include: developing explainable AI models for improved lesion detection, segmentation, and differential diagnosis; employing deep learning techniques for direct image reconstruction and artifact reduction; integrating multiscale data such as imaging, genomic, and clinical information for personalized diagnostics; optimizing nanoprobe design using AI-driven predictive modeling; implementing automated image preprocessing and quality control to enhance reproducibility; establishing standardized data fusion protocols and software platforms for seamless multimodal image integration; engineering real-time multimodal imaging systems for simultaneous acquisition and processing; and designing multifunctional hybrid nanoprobes compatible with multiple imaging modalities to improve diagnostic accuracy and clinical workflow efficiency.

4.6. Expanded applications beyond oncology

While much of the current research focuses on cancer diagnostics, the future of molecular imaging (nano)probes will likely extend to a broader range of medical applications. This includes the detection and monitoring of cardiovascular diseases, infectious diseases, neurological disorders, and metabolic conditions. As researchers develop probes targeting various pathophysiological processes, the versatility of these tools will expand, addressing diverse healthcare needs.

4.7. Global accessibility and implementation

Efforts to increase the accessibility of molecular imaging (nano) probes will be a priority in the coming years. This includes developing cost-effective manufacturing processes and establishing partnerships with healthcare providers to ensure that these advanced diagnostic tools are available to a wider population. As global health initiatives focus on reducing disparities in healthcare access, the implementation of molecular imaging (nano)probes can contribute to improved diagnostics in underserved regions.

5 Conclusion

The advancements in molecular imaging (nano)probes have significantly transformed the landscape of medical diagnostics, providing clinicians with innovative tools to visualize and understand complex biological processes at unprecedented resolutions. The integration of nanotechnology into the design of imaging probes has led to the development of highly specific and sensitive agents that can target particular biomarkers associated with diseases, especially in oncology. Techniques such as magnetic resonance, CT, fluorescence, photoacoustic, and PET imaging have seen substantial improvements, resulting in enhanced detection capabilities and real-time monitoring of treatment responses. These innovations not only facilitate better disease characterization but also play a crucial role in guiding therapeutic decisions, ultimately contributing to the shift towards personalized medicine. Despite the remarkable progress, several challenges persist that can hinder the broader implementation of molecular imaging probes in clinical settings. Issues such as tissue autofluorescence can obscure signals from fluorescent agents, complicating image interpretation and reducing diagnostic accuracy. Furthermore, the limited penetration depth of certain imaging modalities can restrict their use in deep-seated tumors or organs. Additionally, safety concerns regarding the potential adverse effects of some contrast agents and the complexities involved in regulatory approval processes pose significant barriers to the widespread acceptance of these advanced imaging techniques. Addressing these challenges is essential for maximizing the clinical utility of molecular imaging. Looking ahead, the future of molecular imaging (nano)probes appears promising, with ongoing research focused on developing next-generation probes that offer improved targeting, biocompatibility/biosafety, brightness, and stability. Innovations in materials science, including the use of multifunctional NPs, hold the potential to enhance imaging capabilities and enable simultaneous therapeutic applications. Moreover, the integration of AI and machine learning into imaging systems can improve image processing and analysis, allowing for more accurate interpretations and better clinical decision-making. By overcoming existing challenges and leveraging emerging technologies, the field of molecular imaging is poised to make significant contributions to medical diagnostics, ultimately leading to improved patient outcomes and the advancement of personalized healthcare strategies.

Data availability

No data was used for the research described in the article.

Author contributions

Meisam Samadzadeh: writing – review & editing; Arezoo Khosravi: writing – review & editing; Atefeh Zarepour: writing – review & editing; Ghazaleh Jamalipour Soufi: supervision, writing – review & editing; Ali Hekmatnia: writing – review & editing; Ali Zarrabi: supervision, writing – review & editing; Siavash Iravani: supervision, conceptualization, writing – review & editing.

Conflicts of interest

Author(s) declare no conflict of interest.

References

1 J. W. Bai, S. Q. Qiu and G. J. Zhang, *Signal Transduction Targeted Ther.*, 2023, **8**, 89.
2 N. MacRitchie, M. Frleta-Gilchrist, A. Sugiyama, T. Lawton, I. B. McInnes and P. Maffia, *Pharmacol. Ther.*, 2020, **211**, 107550.
3 M. Du, T. Wang, Y. Yang, F. Zeng, Y. Li and Z. Chen, *Contrast Media Mol. Imaging*, 2022, **2022**, 5473244.
4 K. T. Chen, *Pharmaceuticals*, 2023, **16**, 1506.
5 G. Jamalipour Soufi, A. Hekmatnia, S. Iravani and R. S. Varma, *ACS Appl. Nano Mater.*, 2022, **5**, 10151–10166.
6 E. B. Ehlerding, P. Grodzinski, W. Cai and C. H. Liu, *ACS Nano*, 2018, **12**, 2106–2121.
7 V. Duclos, A. Iep, L. Gomez, L. Goldfarb and F. L. Besson, *Int. J. Mol. Sci.*, 2021, **22**, 4159.
8 D. Hussain, N. Abbas and J. Khan, *Bioengineering*, 2024, **11**, 1213.
9 F. Gao, F. Liu, J. Wang, J. Bi, L. Zhai and D. Li, *J. Cancer Res. Clin. Oncol.*, 2024, **150**, 118.
10 J. Bonlawar, A. Setia, R. R. Challa, B. Vallamkonda, A. K. Mehata, Vaishali, M. K. Viswanadh and M. S. Muthu, *Nanotheranostics*, 2024, **8**, 401–426.
11 A. M. Wu, *Methods*, 2014, **65**, 139–147.
12 N. Dammes and D. Peer, *Theranostics*, 2020, **10**, 938.
13 P. Zhang, Y. Cui, C. F. Anderson, C. Zhang, Y. Li, R. Wang and H. Cui, *Chem. Soc. Rev.*, 2018, **47**, 3490–3529.
14 S. Lee, J. Xie and X. Chen, *Biochemistry*, 2010, **49**, 1364–1376.
15 M. Liu, Z. Wang, T. Tan, Z. Chen, X. Mou, X. Yu, Y. Deng, G. Lu and N. He, *Theranostics*, 2018, **8**, 5772.
16 J. Zhang, L. P. Smaga, N. S. R. Satyavolu, J. Chan and Y. Lu, *J. Am. Chem. Soc.*, 2017, **139**, 17225–17228.
17 W. Song, Y. Song, Q. Li, C. Fan, X. Lan and D. Jiang, *Eur. J. Nucl. Med. Mol. Imaging*, 2022, **49**, 2544–2559.
18 S. Pan, A. Ding, Y. Li, Y. Sun, Y. Zhan, Z. Ye, N. Song, B. Peng, L. Li and W. Huang, *Chem. Soc. Rev.*, 2023, **52**, 5706–5743.
19 H.-H. Han, H. Tian, Y. Zang, A. C. Sedgwick, J. Li, J. L. Sessler, X.-P. He and T. D. James, *Chem. Soc. Rev.*, 2021, **50**, 9391–9429.
20 Y. Liu, L. Nie and X. Chen, *Trends Biotechnol.*, 2016, **34**, 420–433.
21 X. Xie Hui, M. O. A. Malik and M. Pramanik, *J. Biomed. Opt.*, 2022, **27**, 070901.
22 X. Wang, Q. Ding, R. R. Groleau, L. Wu, Y. Mao, F. Che, O. Kotova, E. M. Scanlan, S. E. Lewis, P. Li, B. Tang, T. D. James and T. Gunnlaugsson, *Chem. Rev.*, 2024, **124**, 7106–7164.
23 T. Gao, C. Xiang, X. Ding and M. Xie, *Heliyon*, 2024, **10**, e38174.
24 J. Ma, R. Sun, K. Xia, Q. Xia, Y. Liu and X. Zhang, *Chem. Rev.*, 2024, **124**, 1738–1861.
25 W. Huang, Y. Yang and D. Ye, *Chin. J. Chem.*, 2023, **41**, 2382–2399.
26 M. Bouché, J. C. Hsu, Y. C. Dong, J. Kim, K. Taing and D. P. Cormode, *Bioconjugate Chem.*, 2019, **31**, 303–314.
27 J. Liu, P. Cheng, C. Xu and K. Pu, *Nat. Biomed. Eng.*, 2025, **9**, 618–637.
28 D. W. Hwang, A. Maekiniemi, R. H. Singer and H. Sato, *Nat. Rev. Genet.*, 2024, **25**, 272–285.
29 J. Wahsner, E. M. Gale, A. Rodríguez-Rodríguez and P. Caravan, *Chem. Rev.*, 2019, **119**, 957–1057.
30 P. Yue, T. Nagendraraj, G. Wang, Z. Jin and G. Angelovski, *Chem. Sci.*, 2024, **15**(48), 20122–20154.
31 P. Yue, T. Nagendraraj, G. Wang, Z. Jin and G. Angelovski, *Chem. Sci.*, 2024, **15**, 20122–20154.
32 V. Catanzaro, C. V. Gringeri, V. Menchise, S. Padovan, C. Boffa, W. Dastrù, L. Chaabane, G. Digilio and S. Aime, *Angew Chem. Int. Ed. Engl.*, 2013, **52**, 3926–3930.
33 S. Aime, F. Fedeli, A. Sanino and E. Terreno, *J. Am. Chem. Soc.*, 2006, **128**, 11326–11327.
34 S. J. Ratnakar, S. Chirayil, A. M. Funk, S. Zhang, J. F. Queiró, C. Geraldes, Z. Kovacs and A. D. Sherry, *Angew Chem. Int. Ed. Engl.*, 2020, **59**, 21671–21676.
35 M. R. Bashir and K. L. Thomas, *Radiology*, 2023, **308**, e231454.
36 J. Lohmeier, R. V. Silva, A. Tietze, M. Taupitz, T. Kaneko, H. Prüss, F. Paul, C. Infante-Duarte, B. Hamm, P. Caravan and M. R. Makowski, *Eur. J. Nucl. Med. Mol. Imaging*, 2022, **49**, 3692–3704.
37 X. Yang, C. Xu, F. Yao, Q. Ding, H. Liu, C. Luo, D. Wang, J. Huang, Z. Li, Y. Shen, W. Yang, Z. Li, F. Yu, Y. Fu, L. Wang, Q. Ma, J. Zhu, F. Xu, X. Cong and W. Kong, *Eur. Heart J.*, 2023, **44**, 1248–1261.
38 C. Quattrociocchi, A. Mangia, S. Aime, V. Menchise and D. Delli Castelli, *Pharmaceuticals*, 2023, **16**, 1301.
39 Y. C. Chen, P. A. Waghorn, I. A. Rosales, G. Arora, D. J. Erstad, N. J. Rotile, C. M. Jones, D. S. Ferreira, L. Wei, R. V. P. Martinez, F. J. Schlerman, J. Wellen, B. C. Fuchs, R. B. Colvin, I. Ay and P. Caravan, *J. Am. Soc. Nephrol.*, 2023, **34**, 1159–1165.
40 Y. Wu, V. Lloveras, A. Morgado, E. Perez-Inestrosa, E. Babaliari, S. Psilodimitrakopoulos, Y. Vida and J. Vidal-

Gancedo, *ACS Appl. Mater. Interfaces*, 2024, **16**, 65295–65306.
41 R. Zhang, K. Lu, L. Xiao, X. Hu, W. Cai, L. Liu, Y. Liu, W. Li, H. Zhou, Z. Qian, S. Wang, C. Chen, J. Zeng and M. Gao, *Front. Bioeng. Biotechnol.*, 2023, **11**, 1279446.
42 Q. Wu, W. Pan, G. Wu, F. Wu, Y. Guo and X. Zhang, *Atherosclerosis*, 2023, **369**, 17–26.
43 C. Jin, X. Luo, X. Li, R. Zhou, Y. Zhong, Z. Xu, C. Cui, X. Xing, H. Zhang and M. Tian, *Cancer*, 2022, **128**, 2704–2716.
44 M. Liu, R. F. Wang, C. L. Zhang, P. Yan, M. M. Yu, L. J. Di, H. J. Liu and F. Q. Guo, *J. Nucl. Med.*, 2007, **48**, 2028–2036.
45 B. I. Reinfeld, M. Z. Madden, M. M. Wolf, A. Chytil, J. E. Bader, A. R. Patterson, A. Sugiura, A. S. Cohen, A. Ali, B. T. Do, A. Muir, C. A. Lewis, R. A. Hongo, K. L. Young, R. E. Brown, V. M. Todd, T. Huffstater, A. Abraham, R. T. O'Neil, M. H. Wilson, F. Xin, M. N. Tantawy, W. D. Merryman, R. W. Johnson, C. S. Williams, E. F. Mason, F. M. Mason, K. E. Beckermann, M. G. Vander Heiden, H. C. Manning, J. C. Rathmell and W. K. Rathmell, *Nature*, 2021, **593**, 282–288.
46 N. Grey, M. Silosky, C. H. Lieu and B. B. Chin, *World J. Gastroenterol.*, 2022, **28**, 1768–1780.
47 P. S. Liu, H. Wang, X. Li, T. Chao, T. Teav, S. Christen, G. Di Conza, W. C. Cheng, C. H. Chou, M. Vavakova, C. Muret, K. Debackere, M. Mazzone, H. D. Huang, S. M. Fendt, J. Ivanisevic and P. C. Ho, *Nat. Immunol.*, 2017, **18**, 985–994.
48 H. Mukai and Y. Watanabe, *Nucl. Med. Biol.*, 2021, **92**, 156–170.
49 K. Kumar and A. Ghosh, *Bioconjugate Chem.*, 2018, **29**, 953–975.
50 B. J. Evans, A. T. King, A. Katsifis, L. Matesic and J. F. Jamie, *Molecules*, 2020, **25**, 2314.
51 L. Zhang, S. Zhang, J. Wu, Y. Wang, Y. Wu, X. Sun, X. Wang, J. Shen, L. Xie, Y. Zhang, H. Zhang, K. Hu, F. Wang, R. Wang and M. R. Zhang, *Mol. Pharm.*, 2023, **20**, 4256–4267.
52 Y. Liu, X. Yao, C. Wang, M. Wang, Y. Wang, M. Ye and Y. Liu, *Nucl. Med. Commun.*, 2021, **42**, 1144–1150.
53 P. Heidari, A. Haj-Mirzaian, S. Prabhu, B. Ataeinia, S. A. Esfahani and U. Mahmood, *J. Nucl. Med.*, 2024, **65**, 1137–1143.
54 Y. Chen, X. Hou, D. Li, J. Ding, J. Liu, Z. Wang, F. Teng, H. Li, F. Zhang, Y. Gu, S. Yu, X. Qian, Z. Yang and H. Zhu, *J. Pharm. Anal.*, 2023, **13**, 367–375.
55 L. Kang, D. Jiang, E. B. Ehlerding, T. E. Barnhart, D. Ni, J. W. Engle, R. Wang, P. Huang, X. Xu and W. Cai, *Mol. Pharm.*, 2018, **15**, 1627–1634.
56 Z. Zeng, Y. Zheng, X. Yan, J. Tao, L. Li, J. Ding, X. n. Sheng, H. Zhu and Z. Yang, *Biomed. Pharmacother.*, 2024, **178**, 117151.
57 T. Wang, Q. Yang, W. Huang, X. Sun, Y. Lei, H. Xu, L. Song, X. Duan, F. Liu, W. Wang, Z. Bao, J. Gao, F. Wang and L. Kang, *J. Med. Chem.*, 2025, DOI: **10.1021/acs.jmedchem.5c01010**.
58 X. Wang, W. Liu, K. Li, K. Chen, S. He, J. Zhang, B. Gu, X. Xu and S. Song, *Eur. J. Nucl. Med. Mol. Imaging*, 2023, **50**, 2606–2620.
59 J. Kretschmer, R. Chiaffarelli, M. Vuozzo, J. Cotton, J. Blahut, J. Ráliš, M. Dračínský, S. Matějková, U. Seeling, A. M. Schmid, A. F. Martins and M. Polasek, *Angew. Chem., Int. Ed.*, 2024, **63**, e202409520.
60 K. Li, W. Liu, H. Yu, J. Chen, W. Tang, J. Wang, M. Qi, Y. Sun, X. Xu and J. Zhang, *J. Clin. Invest.*, 2024, **134**, e170490.
61 M. D. Farwell, R. F. Gamache, H. Babazada, M. D. Hellmann, J. J. Harding, R. Korn, A. Mascioni, W. Le, I. Wilson, M. S. Gordon, A. M. Wu, G. A. Ulaner, J. D. Wolchok, M. A. Postow and N. Pandit-Taskar, *J. Nucl. Med.*, 2022, **63**, 720–726.
62 S. Kong, Q. Liu, Y. Chen, B. Liang, Y. Zhou, J. Lin, M. Xie and L. Qiu, *Mol. Pharm.*, 2024, **21**, 255–266.
63 A. So and S. Nicolaou, *Korean J. Radiol.*, 2021, **22**, 86–96.
64 H. K. Gaikwad, D. Tsvirkun, Y. Ben-Nun, E. Merquiol, R. Popovtzer and G. Blum, *Nano Lett.*, 2018, **18**, 1582–1591.
65 L. Feng, W. Hu, X. Zeng, Z. Wei, Y. Long, M. Li, S. Sun, Z. Guo, X. Lan and X. Zhang, *Mol. Pharm.*, 2024, **21**, 4386–4394.
66 X. Wen, X. Zeng, J. Liu, X. Zeng, Y. Zhang, X. Cheng, J. Huang, Y. Li, R. Zhuang, X. Zhang and Z. Guo, *Bioconjugate Chem.*, 2023, **34**, 2387–2397.
67 B. Gu, Z. Yang, X. Du, X. Xu, X. Ou, Z. Xia, Q. Guan, S. Hu, Z. Yang and S. Song, *J. Nucl. Med.*, 2024, **65**, 365–371.
68 A. Dickhout, P. Van de Vijver, N. Bitsch, S. J. van Hoof, S. Thomassen, S. Massberg, P. Timmerman, F. Verhaegen, R. R. Koenen, I. Dijkgraaf and T. M. Hackeng, *Biomolecules*, 2022, **12**(6), 829.
69 A. P. G. Walsh, E. Yu, J. D. McFadyen, V. Bongcaron, M. J. Moon, A. Huang, J. F. Arthur, I. L. Muir, V. Rayzman, C. Panousis, X. Wang and K. Peter, *Arterioscler., Thromb., Vasc. Biol.*, 2023, **43**, 1031–1040.
70 L. Hou, H. Zhang, Y. Li, H. Zhu, K. Liao, B. Guo, C. Dong, G. Li, W. Ye, L. Wang and H. Xu, *Quant. Imag. Med. Surg.*, 2023, **13**, 7924–7935.
71 S. Fayn, A. P. King, N. T. Gutsche, Z. Duan, J. Buffington, C. P. Olkowski, Y. Fu, J. Hong, D. Sail, K. E. Baidoo, R. E. Swenson, R. W. Cheloha, M. Ho, P. L. Choyke and F. E. Escorcia, *J. Nucl. Med.*, 2023, **64**, 1017–1023.
72 J. Du, S. Yang, Y. Qiao, H. Lu and H. Dong, *Biosens. Bioelectron.*, 2021, **191**, 113478.
73 C. He, J. Zhu, H. Zhang, R. Qiao and R. Zhang, *Biosensors*, 2022, **12**(11), 947.
74 O. Santos, J. Cancino-Bernardi, P. M. Pincela Lins, D. Sampaio, T. Pavan and V. Zucolotto, *ACS Appl. Bio Mater.*, 2021, **4**, 6780–6790.
75 C. Liu, X. Zheng, T. Dai, H. Wang, X. Chen, B. Chen, T. Sun, F. Wang, S. Chu and J. Rao, *Angew Chem. Int. Ed. Engl.*, 2022, **61**, e202116802.
76 L. Ni, X. Wang and G. Xu, *Z. Med. Phys.*, 2023, **33**, 324–335.
77 J. Jo, G. Xu, E. Schiopu, D. Chamberland, G. Gandikota and X. Wang, *J. Biomed. Opt.*, 2020, **25**(12), 126005.
78 M. Biniecka, M. Canavan, T. McGarry, W. Gao, J. McCormick, S. Cregan, L. Gallagher, T. Smith, J. J. Phelan, J. Ryan, J. O'Sullivan, C. T. Ng, D. J. Veale and U. Fearon, *Ann. Rheum. Dis.*, 2016, **75**, 2192–2200.

79 M. Miao, J. Miao, Y. Zhang, J. Zhang, M. She, M. Zhao, Q. Miao, L. Yang, K. Zhou and Q. Li, *Biosens. Bioelectron.*, 2023, **235**, 115399.
80 Y. Pan, J. Chen, Y. Zhang, Y. Ren, Z. Wu, Q. Xue, S. Zeng, C. Fang, H. Zhang, L. Zhang, C. Liu and J. Zeng, *Mol. Pharm.*, 2024, **21**, 1804–1816.
81 X. Hu, X. Sun, X. Liu, H.-D. Xu, L. Yang, S. Liu, R. Wang and G. Liang, *Anal. Chem.*, 2023, **95**, 14511–14515.
82 M. Li, N. Beaumont, C. Ma, J. Rojas, T. Vu, M. Harlacher, G. O'Connell, R. C. Gessner, H. Kilian, L. Kasatkina, Y. Chen, Q. Huang, X. Shen, J. F. Lovell, V. V. Verkhusha, T. Czernuszewicz and J. Yao, *IEEE Trans. Med. Imaging*, 2022, **41**, 2704–2714.
83 J. G. de Wit, J. Vonk, F. J. Voskuil, S. de Visscher, K. P. Schepman, W. T. R. Hooghiemstra, M. D. Linssen, S. G. Elias, G. B. Halmos, B. E. C. Plaat, J. J. Doff, E. L. Rosenthal, D. Robinson, B. van der Vegt, W. B. Nagengast, G. M. van Dam and M. J. H. Witjes, *Nat. Commun.*, 2023, **14**, 4952.
84 Q. Liu, J. Huang, L. He, X. Yang, L. Yuan and D. Cheng, *Chem.–Asian J.*, 2022, **17**, e202200091.
85 Y. Kang, X. Zhai, S. Lu, I. Vuletic, L. Wang, K. Zhou, Z. Peng, Q. Ren and Z. Xie, *Front. Oncol.*, 2022, **12**, 772392.
86 R. Ito, M. Kamiya and Y. Urano, *Curr. Opin. Chem. Biol.*, 2022, **67**, 102112.
87 H. Li, Q. Yao, W. Sun, K. Shao, Y. Lu, J. Chung, D. Kim, J. Fan, S. Long and J. Du, *J. Am. Chem. Soc.*, 2020, **142**, 6381–6389.
88 W. Yang, P. K. Srivastava, S. Han, L. Jing, C. C. Tu and S. L. Chen, *Anal. Chem.*, 2019, **91**, 5499–5503.
89 T. Kim, W. S. Lee, M. Jeon, H. Kim, M. Eom, S. Jung, H. J. Im and S. J. Ye, *Med. Phys.*, 2023, **50**, 529–539.
90 D. Li, Q. Liu, Q. Qi, H. Shi, E. C. Hsu, W. Chen, W. Yuan, Y. Wu, S. Lin, Y. Zeng, Z. Xiao, L. Xu, Y. Zhang, T. Stoyanova, W. Jia and Z. Cheng, *Small*, 2020, **16**, e2003851.
91 F. Azari, G. Kennedy, E. Bernstein, J. Delikatny, J. Y. Lee, J. Kucharczuk, P. S. Low and S. Singhal, *Mol. Imaging Biol.*, 2023, **25**, 85–96.
92 T. Nagaya, Y. A. Nakamura, P. L. Choyke and H. Kobayashi, *Front. Oncol.*, 2017, **7**, 314.
93 M. Miampamba, J. Liu, A. Harootunian, A. J. Gale, S. Baird, S. L. Chen, Q. T. Nguyen, R. Y. Tsien and J. E. González, *Theranostics*, 2017, **7**, 3369.
94 R. Zhou, C. Wang, X. Liang, F. Liu, P. Sun, X. Yan, X. Jia, X. Liu, Y. Wang and G. Lu, *Theranostics*, 2023, **13**, 95–105.
95 J. Wei, K. Zhu, Z. Chen, Z. Yang, K. Yang, Z. Wang, S. Zong and Y. Cui, *Microchim. Acta*, 2022, **189**, 182.
96 X. Zhang, P. Wang, G. Shi, C. Tang and H. Xue, *Bioconjugate Chem.*, 2024, **35**, 1064–1074.
97 J. R. M. Ferreira, M. Alves, B. Sousa, S. I. Vieira, A. M. S. Silva, S. Guieu, Â. Cunha and R. Nunes da Silva, *Org. Biomol. Chem.*, 2023, **21**, 1531–1536.
98 B. Wang, C. Tang, E. Lin, X. Jia, G. Xie, P. Li, D. Li, Q. Yang, X. Guo and C. Cao, *EBioMedicine*, 2023, **98**, 104880.
99 I. C. Mondal, P. Rawat, M. Galkin, S. Deka, A. Karmakar, P. Mondal and S. Ghosh, *Org. Biomol. Chem.*, 2023, **21**, 7831–7840.
100 C. Zhang, H. Cheng, S. Dou, Y. Wang, X. Ye, H. Cui, X. Chang and Y. Li, *J. Ovarian Res.*, 2024, **17**, 225.
101 S. Kang, H. Ahn, C. Park, W. H. Yun, J. G. Jeong, Y. J. Lee and D. W. Kim, *Advanced Science*, 2023, **10**, 2300462.
102 M. Kumar, S. Chinnathambi, N. Bakhori, N. Abu, F. Etezadi, V. Thangavel, D. Packwood, E. Sivaniah and G. N. Pandian, *Sci. Rep.*, 2024, **14**, 12665.
103 Y.-F. He, K. Cheng, Z.-T. Zhong, X.-L. Hou, C.-Z. An, J. Zhang, W. Chen, B. Liu, J. Yuan and Y.-D. Zhao, *Anal. Chim. Acta*, 2023, **1260**, 341210.
104 J. Wahsner, E. M. Gale, A. Rodríguez-Rodríguez and P. Caravan, *Chem. Rev.*, 2018, **119**, 957–1057.
105 J. Trotter, A. R. Pantel, B. K. Kevin Teo, F. E. Escorcia, T. Li, D. A. Pryma and N. K. Taunk, *Adv. Radiat. Oncol.*, 2023, **8**, 101212.
106 R. Najjar, *iRadiology*, 2024, **2**, 430–468.
107 I. Steinberg, D. M. Huland, O. Vermesh, H. E. Frostig, W. S. Tummers and S. S. Gambhir, *Photoacoustics*, 2019, **14**, 77–98.
108 B. Sridharan and H. G. Lim, *J. Nanobiotechnol.*, 2023, **21**, 437.
109 M. Koch, P. Symvoulidis and V. Ntziachristos, *Nat. Photonics*, 2018, **12**, 505–515.
110 H. Hricak, M. E. Mayerhoefer, K. Herrmann, J. S. Lewis, M. G. Pomper, C. P. Hess, K. Riklund, A. M. Scott and R. Weissleder, *Lancet Oncol.*, 2025, **26**, e34–e45.
111 G. Jamalipour Soufi and S. Iravani, *Green Chem.*, 2020, **22**, 2662–2687.
112 C. Yin, P. Hu, L. Qin, Z. Wang and H. Zhao, *Int. J. Nanomed.*, 2024, **19**, 9549–9574.
113 W. Sun, G. Tian and L. Lu, *Analysis Sensing*, 2023, **3**, e202300038.
114 H. He, X. Zhang, L. Du, M. Ye, Y. Lu, J. Xue, J. Wu and X. Shuai, *Adv. Drug Delivery Rev.*, 2022, **186**, 114320.
115 A. V. Singh, P. Bhardwaj, A. K. Upadhyay, A. Pagani, J. Upadhyay, J. Bhadra, V. Tisato, M. Thakur, D. Gemmati, R. Mishra and P. Zamboni, *Explor. BioMat-X*, 2024, **1**, 124–134.
116 C. Yin, P. Hu, L. Qin, Z. Wang and H. Zhao, *Int. J. Nanomed.*, 2024, **19**, 9549–9574.
117 J. M. Metselaar and T. Lammers, *Drug Delivery Transl. Res.*, 2020, **10**, 721–725.
118 R. Jin, X. Fu, Y. Pu, S. Fu, H. Liang, L. Yang, Y. Nie and H. Ai, *Adv. Drug Delivery Rev.*, 2022, **191**, 114587.
119 S. Hua, M. B. C. de Matos, J. M. Metselaar and G. Storm, *Front. Pharmacol*, 2018, **9**, 790.